Resistive Embedded Heating for Homogeneous Curing of Composite Damage Repair

Mahdi Ashrafi

A dissertation submitted in fulfillment of the
requirements for the degree of

Doctor of Philosophy

University of Washington

2016

Reading Committee:

Mark Tuttle, Chair

Santosh Devasia, Chair

Jinkyu Yang

Program Authorized to Offer Degree:
Mechanical Engineering

University of Washington

Abstract

Resistive Embedded Heating for Homogeneous Curing
of Composite Damage Repair

Mahdi Ashrafi

Co-Chairs of the Supervisory Committee:
Prof. Mark Tuttle
Department of Mechanical Engineering

Prof. Santosh Devasia
Department of Mechanical Engineering

The increased use of composite materials in passenger aircrafts has resulted in an escalation of maintenance issues associated with composite structure damage from a variety of causes including impacts during towing, bird strikes and hail. Hence, damage repair has become an important issue in the aerospace industry. This research aims to improve the performance of current composite repair technology by direct application of heat using an embedded heater in the bondline between the base laminate and the repair material rather than the use of surface heating such as using heatlamps or heat blankets. The use of surface heating can lead to large thermal gradients potentially resulting in improper cure. The proposed embedded heating can: (i) avoid large thermal gradients; (ii) lead to a more uniform cure of the adhesive during repair; (iii) improve performance metrics, including increased strength, stiffness; and (iv) reduce or eliminate thermal warping of the repaired structure. The goal of the proposed research is to enable an energy-efficient, adhesive-bonding approach for joining carbon-fiber composite components, which can lead to a new direction for advanced composites manufacturing. By localizing the heating to where it is needed, the proposed approach can substantially reduce the energy and cost of joining composite components, when compared to the use of traditional methods such as using autoclaves.

ACKNOWLEDGMENTS

Firstly, I would like to express my sincere gratitude to my advisers, Prof. Mark Tuttle and Prof. Santosh Devasia for their continuous support of my Ph.D study and related research. Their mentorship and guidance, while letting me to think freely had led me to be ever more passionate and dedicated to my Ph.D research. Their immense knowledge have not only helped me to learn more, but also to grow professionally. I could not have imagined having a better team of co-advisers and mentors for my Ph.D study.

Besides my advisers, I would like to thank the rest of my thesis committee: Dr. Jinkyu Yang and Dr. Brian Flinn for their insightful comments and encouragement, but also for the hard question which motivated me to widen my research from various perspectives.

My sincere thanks also goes to the staff in the Mechanical Engineering department, specially, Mr. Bill Kuykendall and Mr. Eamon McQuaide who helped me with training and various machining projects.

I thank all of my current and previous labmates and researchers that I have worked with over the past four years. In particular, Brandon Smith whom has been working closely with me on this project. Additionally, I want to thank Dr. Gun-In Kim, Dr. Scott Wilcox, Dr. Teymoor Javaherchi, Karen Harban, Jonathan Realmuto, Nathan Banka, Arom Boekfah, Rahul Warrier, Parker Owan, Saad Zaki, and Rose Hendrix for the stimulating discussions, for the sleepless nights we were working together before deadlines, and for all the fun we have had in the last four years.

Last but not the least, I would like to thank my family: my parents Dr. Dariush Ashrafi and Mrs. Shahla Rafiee, and my sister Dr. Maedeh Ashrafi for their unconditional love and support through this journey.

This work was partially funded by the US National Science Foundation under Grant Award# CMMI 1536306, and I wanted to thank them for providing the financial support to complete

this research.

DEDICATION

This dissertation is gratefully dedicated to my parents, Dariush and Shahla, for their endless love, support, and encouragement.

TABLE OF CONTENTS

LIST OF FIGURES

Chapter 1

INTRODUCTION

Carbon fiber reinforced plastics (CRFPs), commonly known as composites, are increasingly becoming integral to a variety of markets such as aerospace, renewable energies, marine, and automotive industries. High strength, low weight, and corrosion resistance make CFRPs ideal for engineering applications in comparison to other materials such as steel and aluminum alloys. Composite materials help to produce lighter weight aircrafts that have improved structural properties, thereby reducing fuel consumption and direct operating costs while improving their efficiency. In particular, the amount of composite materials that are used in a commercial aircraft is 10 times more than 25 years ago, and it is projected that nearly 50% of every aircraft manufactured by 2020 will be made out of composite materials [1]. Additionally, in alternative energy industries, composites are used to increase efficiency of wind turbines by enabling manufacturers to produce larger blade rotors. Large wind turbines are estimated to account for about 70% of wind turbine industry production [2].

The goal of the proposed project is to commercialize an effective and energy-efficient, adhesive-bonding approach for joining CFRP composite components, which can lead to a new direction for advanced composites manufacturing and repair. Furthermore, this project aims to improve the performance of the current composite repair technology by direct application of heat using an embedded heater in the bond-line between the base laminate and the repair material, rather than the traditional use of surface heating that is prevalent in the market today. Current use of surface heating leads to large thermal gradients resulting in improper cure [3, 4]. The proposed embedded heating can: (i) avoid large thermal gradients; (ii) lead to a more uniform cure of the adhesive during repair; (iii) reduce or eliminate over-heating and thermal warping of the repaired structure; and (iv) reduce the energy and cost of joining composite components, when compared to the use of autoclaves/ovens.

1.1 Research Goal

The goal of the proposed research is to enable an energy-efficient, adhesive-bonding approach for joining high-strength (carbon-fiber) composite components, which can lead to a new direction for advanced composites manufacturing and repair. At present, a common requirement is to rapidly repair a composite structure without removing it from the aircraft. Repair of thick structures while still on the aircraft can be difficult to achieve. For example, the thermal energy necessary to cure the repair adhesive must diffuse through the composite layers to reach the joint repair interfaces, resulting in long and expensive processing times as well as wasted energy [5, 6, 7, 8] .Rather than heat the entire system to cure the adhesive, this research will investigate controlled heating targeted at the bond-line with an embedded heater. By localizing the heating to where it is needed, the proposed approach can substantially reduce the energy and cost of joining composite components, when compared to the use of autoclaves. Figure 1.1 shows an embedded heater applies heat at the bondline rather than through multiple fabrics on the surface, reducing through thickness gradients in comparison with the surface heating method.

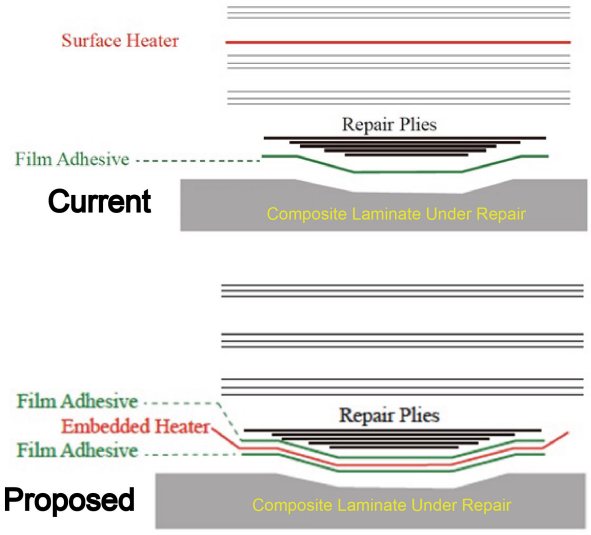

Figure 1.1: A comparison between heat delivery in the proposed vs. current approaches

1.2 Research Challenges

1.2.1 Adding carbon-fiber fabric in the bond-line

Adding carbon-fiber fabric in the bond results in increasing the bond-line thickness and stiffness; therefore, it is essential to study the mentioned effects on the mechanical performance of the bond. One of the issues raised by this is to understand the effect of adding an additional fabric on the bond strength by measuring the strain induced in the bond as a result of loading. A difficulty in measuring strains is the small bond-line thickness. Therefore, contact methods such as utilizing strain gauges cannot be used with such small dimensions [9]. We propose to use non-contact methods to obtain the bond-line strains. In particular, digital image correlation (DIC) can provide full-field displacements and strains. Additionally, theoretical and Finite Element (FE) models could also be used to predict the effect of adding embedded-fabric and adhesive-film on the joint strength.

1.2.2 Repairing large areas

Applying the proposed method to the real-life conditions might include repairs with large areas and multiple heat-sinks. Therefore, it is essential to ensure that the embedded heater is capable of generating proper heat for curing the bond area. To address this issue, it is possible to use multiple, parallel embedded carbon-fiber meshes, with separate heaters to achieve the desired cure temperature for large areas as shown in Figure 1.2. Another challenge is the dependency of the heat generated by the proposed method on the electrical resistance and geometry of the carbon fiber mesh. Thus, it is required to evaluate the heat generation capability of the embedded heater through FE models and/or experimentally by completion of a dry-run test prior to starting the repair process.

1.2.3 Maintaining uniform temperature in presence of heat-sinks/substructures

Surrounding structures in contact with the internal surface (e.g., stringers or frames) are often present and act as heat sinks, generally increasing both through-thickness and in-plane thermal gradients. Therefore, another challenge in this research is to achieve uniform temperature in the bond-line in presence of uneven heat-loss distribution, e.g., due to structures

Figure 1.2: Using multiple heaters to achieve the desired temperature in the bond-line

adjacent to the bond-line. Subsequently, a model based optimization of multiple heater sections is proposed to account for varying thermal conduction characteristics and achieving a more uniform temperature distribution.

1.3 Research Impacts

The life cycle costs and sustainability are improved if the useful life of large composite structures can be extended by repairing occasional damage. Currently single-sided composite patches are used for aircraft repair [10]. Typically heat is applied from the external surface, e.g., using heat blankets or heat lamps to cure the adhesive at the bond-line. However, due to the relatively low thermal conductivity of the composites involved, the approach of heating the adhesives by using heating elements placed on the outer surfaces invariably leads to throughthickness thermal gradients. That is, the temperatures induced at the surface can be significantly higher than at subsurface locations where the bond-line is located. Moreover, surrounding structures (e.g., stringers or frames) often act as heat sinks, generally increasing both through-thickness and in-plane thermal gradients. Structural film adhesives are typically cross-linking thermosets (e.g., epoxies) and require precise control of the temperature profile (both spatial and temporal) to cure properly. Thus, the thermal gradients induced by standard surface heating techniques can lead to improperly-cured ad-

hesive, resulting in low bond-line strength and/or stiffness and an unacceptable joint. The proposed embedded heating approach can improve the control of bond-line temperatures and therefore improve the adhesive-bonding of repair patches, and extend the useful life of relatively-large, composite structures.

1.4 Broader Impacts

1.4.1 Adhesive bonding can reduce manufacturing cost

An alternate approach to reduce the prohibitive cost of large autoclaves is to fabricate smaller parts and then join them. This approach is taken, for example, in the assembly of the fuselage sections of Boeing 787 Dreamliner and the Airbus A350XWB. The fuselage is made of high-strength CFRP composite sections that are produced in autoclaves and then joined together. Nevertheless, at present, such joining operation is expensive as it requires time-and-labor intensive drilling of holes for fasteners [11, 12]. An alternative approach is to bond the composite parts together, which would typically require an even larger autoclave to heat the entire system. Therefore, the proposed energy efficient, adhesive-bonding approach to join composites (without an autoclave) can have a substantial impact on reducing the manufacturing cost for large, high-strength, CFRP composite structures.

1.4.2 Reducing manufacturing cost can open new markets

Carbon fibre reinforced polymer (CFRP) composites with a thermoset resin such as epoxy can lead to some of the highest strength-to-weight ratio and rigidity. Therefore, CFRPs have been used in aerospace, sailing boats, and top-end bicycles, cars and motorcycles. In modern aerospace industry more than 50% by weight of the aircraft is made of composites. However, in addition to the high cost of the carbon fibers, the need to use autoclaves to cure the thermoset resin implies that these composites can be expensive to manufacture. In particular, the cost of manufacturing with autoclaves tends to be prohibitive as the size of the part increases in applications such as wind-turbines since the renewable-energy industry is very sensitive to the cost of energy. Although out-of-autoclave processes [13, 14] such as vacuum-assisted resin transfer molding (VARTM) with low temperature cure epoxy resins

[15, 16] have been developed, it is challenging to extend these methods to manufacture higher strength-to-weight-ratio composites, which require higher cure temperatures [17]. Nevertheless, as the turbine blades become increasingly large, there is increasing interest in using high-strength CFRPs provided the manufacturing cost can be reduced. Hence, reducing the manufacturing cost of high strength composites can directly impact their wider use to improve the performance of societally-important applications.

1.5 Research Path and Dissertation Structure

The research discussed here has been broken up into three parts:

1. This research will first focus on implementation and evaluation issues to demonstrate technical feasibility of the proposed embedded heating approach on Single Lap Joints (SLJs). Shear lap testing results have shown that the average joint performance where the adhesive was cured using embedded resistive heating was similar or higher than the samples cured using conventional techniques. This work was published in International Journal of Adhesion & Adhesives [5]. This article is contained in chapter 2.

2. After demonstrating the feasibility of the proposed approach, composite scarf repair specimens were created using the embedded heating approach, and through the use of a heat blanket for circular and rectangular scarf configurations. By heating the bondline directly, instead of heating the entire structure, it was shown that this method achieved relatively uniform temperatures in the bondline, while avoiding possible overheating of the surface adjacent to the repair, which may occur when heat is applied using an external heater. The above targets where achieved without jeopardizing the structural performance of the repair. This work [18] was submitted to be published in Journal of Composites - Part A in February 2016. This article is presented in chapter 3.

3. A detailed Finite Element study was completed to study different factors such as the embedded heater geometry, number of electrical inputs, heatsinks, and insulation on

the temperature uniformity of the embedded heater. The results were initially compared to experimental measurements using temperature sensors and a thermal camera. This work is included in chapter 4.

The embedded resistive heating approach could be combined with external heating to maintain uniform temperatures across the repair area rather than solely in the bondline in the cases that B-staged repair plies are cured along with the thin film adhesive. This idea is presented in chapter **??** as potential future continuation to this work.

The conclusions of the work presented are in chapter 5 and Appendices include a modified version of Goland and Reissner solution for SLJs, Finite Element study of the single lap joint model, the heat diffusion equation, and curing scarf repairs with B-staged repair plies.

Chapter 2

RESISTIVE EMBEDDED HEATING FOR HOMOGENEOUS CURING OF ADHESIVELY BONDED JOINTS

To evaluate the new curing approach, SLJs were produced using embedded resisitive heating technique, and were compared to the specimens produced by conventional methods such as using autoclaves and ovens to cure bonded joints.

Adding carbon fiber fabric in the bond-line significantly changes the stress distribution by changing the effective stiffness and total thickness. To study the mentiond effects, stress distribution in the bond-line was studied using a simple Finite element (FE) model as well as a closed-form theoretical solution by Goland & Reissner [19] which was modified to account for the change in adherends' Poisson's ratio. Details of the closed-form solution and FE study are presented in Appendix A and Appendix B.

2.1 History and Background

A common requirement is to rapidly repair a composite structure without removing it from the aircraft. Repair of thick structures while still on the aircraft can be difficult to achieve. For example, the thermal energy necessary to cure the repair adhesive must diffuse through the composite layers to reach the joint repair interfaces, resulting in long and expensive processing times as well as wasted energy [6, 7, 8]. Surrounding heat-sensitive materials or equipment may also be damaged. The most popular approach is to use a surface heater such as heat blanket(s) and/or heat lamps to generate the heat needed to cure the repair adhesive. In these approaches the entire structure is heated to initiate cure of the repair adhesive, typically a high-strength thermoset such as an epoxy. CFRPs typically exhibit poor thermal conductivities and consequently the temperature of the heated surface can be much higher than the temperature at the subsurface repair bondline. Large thermal gradients are inevitably created, resulting in an inefficient repair process.

In the past literature, efforts have been reported to reduce the cost of producing ther-

moset/thermoplastic composites by avoiding the need for expensive autoclaves or ovens. These methods could conceptually be used during composite repair, as discussed in reference [7]. As a case in point, UV photo-curable adhesives were utilized in the past and cured through transmission of the UV light through the laminate [20, 21]. Microwave curing of composite materials has been considered as a highly efficient volume-heating radiation manufacturing process; however, heating efficiency of the microwave depends greatly on the dielectric properties of the material [22, 23]. Inductive heating or welding has proven to be effectively employed in an epoxy adhesive between composite adherends to cure the bond and produce strong joints [6, 24]. Nonetheless there are difficulties associated with edge and local heating effects that have limited large scale applications [7, 24, 25, 26]. In the past literature, resistive heating has been used in CFRP processing in order to increase energy efficiency and reduce curing time/cost. Some references used one or multiple carbon-fiber mesh (es) as resistive heaters to provide the necessary heat to create composite parts [27, 26, 28, 29, 30] . Specifically, reference [31] used carbon fiber as a heating element to produce CFRP laminates using vacuum assisted infusion molding. Moreover, reference [32] used aligned carbon nanotube film as an external resistive heater to cure a composite laminate sample. In contrast, some researchers have utilized the carbon fibers that are already embedded in the prepregs and intrinsic to the structure as the heating element instead of introducing a new carbon fabric mesh to be used as the heater [33, 34, 35, 36, 37]. Although there are many studies available in the literature for resistive heating in processing composite structures, utilizing this method for curing structural adhesive films were only highlighted in few works in the past. Rider et al. [7] reported the use of a stainless steel mesh as an embedded resistive heater to achieve shear strength similar to the joints cured by the conventional methods; however, shear strength was proven to be highly dependent on the stainless steel mesh surface treatment. Additionally, references [5, 38, 39] used dry carbon fabric for bonding CFRPs. Mas et al. and Sung et al.[40, 41] also utilized fabrics that were made from Carbon Nanotubes (CNTs) to join CFRP parts. Resistive heating in bonding applications is a relatively new technique, and very few studies are available in the literature.

We propose to achieve a bonded repair by passing an electric current through a carbon

fiber fabric sandwiched between two layers of structural adhesive film and embedded in the repair bondline. The carbon fabric serves as an embedded a resistance heater. A substantial advantage of this approach is that the carbon fibers that initially serve as heating elements remain in the bondline as reinforcing materials. Many types of carbon fibers have already been certified for use in transport aircraft (e.g., AS4 or IM7 fibers), which could facilitate certification of the proposed approach for use in commercial aircraft. The epoxy adhesive electrically insulates the embedded heater from the electrically conductive adherends. Moreover, it will be shown that bonded joints cured via an embedded resistive heating method have single-lap shear strengths comparable to the strengths of samples cured in an autoclave.

2.2 Experimental Study

In this section, an experimental investigation examining the cure of a thermoset adhesive film between carbon composite adherends by using resistive heating of an embedded carbon fiber mesh is described. It is shown that the method is energy-efficient and results in low temperature gradients due to the negligibly small distance between the heat source and the repair bondline. The technique could be applied to large scale composite repairs, or possibly employed during original manufacture of a bonded composite structure.

2.2.1 Materials

The single-lap joint specimens were fabricated using composite panels manufactured using Toray carbon/epoxy prepreg (T800-HB-12K-40B) with $[0/+45/90/-45]_s$ quasi-isotropic stacking sequence and cured in autoclave according to the curing cycle suggested by the prepreg manufacturer (1.66 °C/min heat-up rate, 130 minutes hold at 176.67 °C with 586 kPa external pressure with vacuum). The composite laminates were then cut to 22.9 cm × 10.2 cm using an abrasive disc. One 22.9 cm edge of each panel was sanded with 240 grit paper, degreased using acetone, and then air dried for two hours.

Unidirectional carbon fabric (Fibre Glast 12K, 0.1524 mm thick) was used as the embedded mesh fabric, and is shown in Figure 2.1A. The fabric was cut to the dimensions depicted in Figure 2.1B. Flash tape was used to electrically insulate the out-of-bond regions of the

embedded fabric from the conductive adherends. Two layers of structural adhesive film

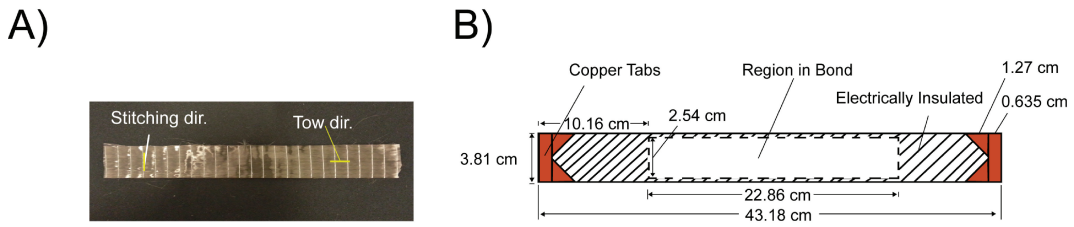

Figure 2.1: A) Uni-directional carbon fiber mesh used as the embedded heater. B) Schematic of the embedded carbon fiber mesh.

(Scotch-Weld AF 163-2U) with 0.0635 mm thickness were used to bond the adherends. The modulus of elasticity, shear modulus, and Poissons ratio of the adhesive were reported by its manufacturer to be 1110 MPa, 414 MPa, and 0.34 at 24 °C respectively. The adhesive films were cut slightly larger than the bonding region to ensure no contact between the embedded fabric and the adherends.

2.2.2 Embedded resistive curing of bonded joints

Carbon/epoxy composite panels are electrically conductive, and can interfere in the resistive heating process in the case of any contact between the embedded fabric and adherends. Therefore prior to any experiments, resistance testing was conducted to ensure complete electrical insulation between the embedded fabric and the composite adherends. In the bond region, a layer of thin adhesive film was placed on each side of unidirectional carbon fabric. As shown in Figure 2.2A a flat plate was used to avoid bending of the top adherend. Several layers of bleeder cloths were used as thermal insulators in order to minimize the transfer of heat to the underlying caul plate during the cure process. Figure 2.2B shows the experimental setup prior to and after insulation and vacuum bagging. Vacuum pressure was applied to the setup prior to the heating process, and was kept at 33.86 kPa until the sample reached the ambient temperature. A proportional-integral-derivative (PID) Controller (Omega CN7500) was connected to a variable voltage convertor. The standard line voltage of 110 V was stepped down to 50 V before applying to the embedded heater for

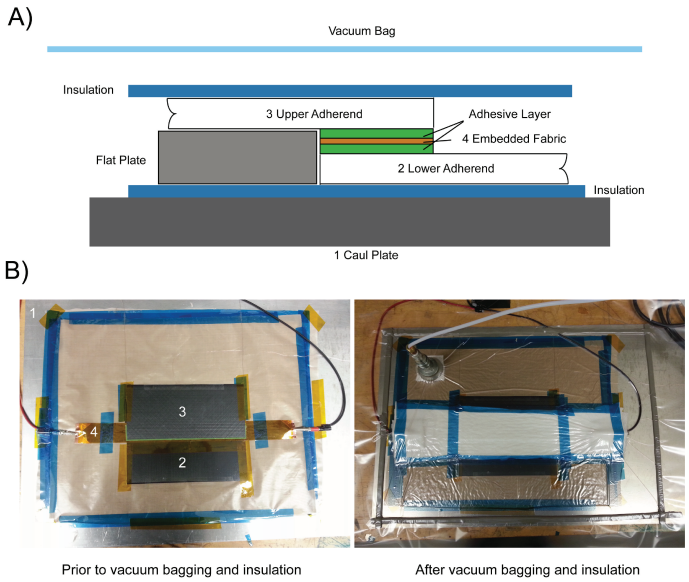

Figure 2.2: A) Schematic of the experimental setup for embedded resistive curing of a single lap joint. B) Photograph of the experimental setup prior to and after vacuum bagging and insulation.

the resistive curing. The end-to-end resistance of the carbon fabric mesh was measured to be 14.5 Ω, and therefore the maximum power generated was approximately 170 W which is considerably lower than the power consumption of a typical autoclave. The PID controller provided control of the power output with a thermocouple input embedded in the middle of the bond to provide temperature feedback a thermal camera (FLIR T-640) was used to monitor the temperature distribution in the bond region, as shown in Figure 2.3A. Figure 2.3B shows that the temperature distribution was relatively uniform along the bond region, which is a desirable condition in any composite repair systems [8]. Furthermore, no local hot spots were observed in the embedded fabric. Hot spots could potentially damage the thin film adhesive through excessive heat. The embedded resistive heating method can also be applied to the larger bond areas with some changes. For example, in cases where the use of an embedded thermocouple is undesirable, the uniform temperature distribution in the embedded fabric (see Figure 2.3B) can enable temperature control using thermocouples outside of the bond area. Additionally, internal temperatures could be estimated using

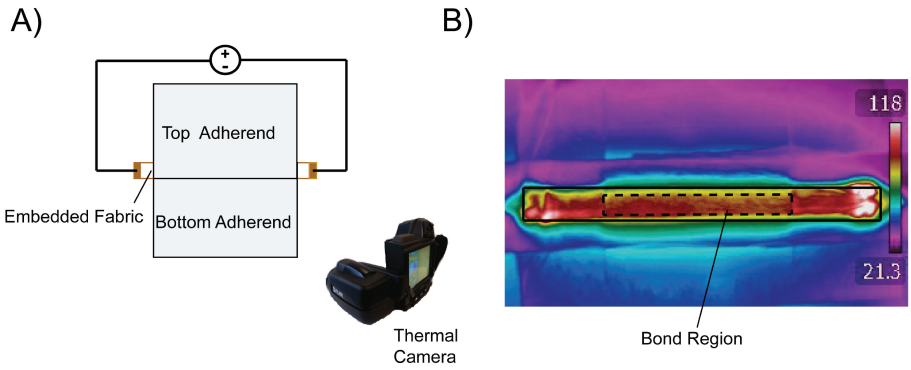

Figure 2.3: A)Schematic of the closed-loop control using an embedded temperature sensor. B) Thermal picture of the bond region shows that the temperature range in the overlap was about 15 °C.

external temperature sensors. Moreover, the amount of the heat produced in the embedded heater depends on the geometry, and the tow size of the carbon fiber mesh, which can be optimized for the bond area. For example, it is possible to use multiple, parallel embedded carbon-fiber meshes, with separate heaters to achieve the desired cure temperature for large areas.

2.2.3 Curing adhesively bonded joints through conventional methods

The shear strength of the bonded joints fabricated using embedded resistive heating was compared to strengths of test samples manufactured in an oven as well as in an autoclave. Vacuum pressure of 33.86 kPa was applied to the oven cured samples. In the autoclave cured samples a 344 kPa overpressure was applied in addition to vacuum pressure, in accordance with the suggested curing pressure from the adhesive manufacturer. Additionally, bonded joints with two layers of adhesive film and without an embedded fabric in the bond were produced to compare with the samples having an embedded mesh inside. Three K-type thermocouples were embedded on the mesh to monitor the temperature inside of the joints. Figure 2.4 shows the location of each thermocouple located in the bond region. Feedback from TC-Middle was used to control temperature during the curing process. Temperature increase rate was 2 °C/min, and temperatures were maintained to at least 120 °C for 1hr, as

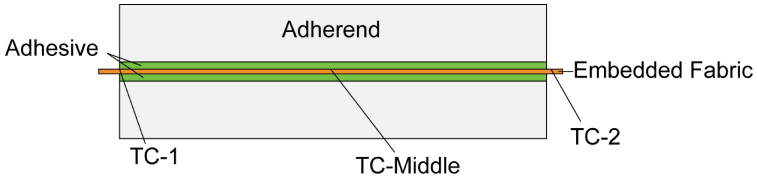

Figure 2.4: Schematic of the bondline showing the location of thermocouples.

shown on Figure 2.5A. Pressures were maintained during cool down to ambient conditions. Figure 2.5B presents the temperature data feedback recorded by all three thermocouples in embedded resistive heating method. Seven single-lap specimens were machined from

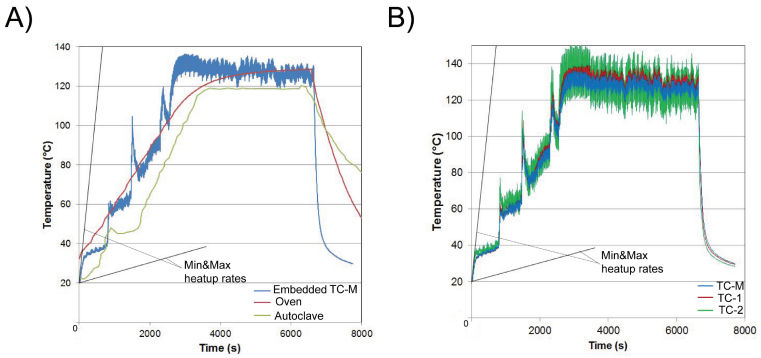

Figure 2.5: A) Temperature feedback for TC-Middle in all three cure processes. B) Temperature feedback for TC-Middle, TC-1, and TC-2 in the embedded resistive heating cure process.

these panels, as shown in Figure 2.6. Specimen width was 25.4 mm. Note that the three thermocouples used to monitor and control bondline temperatures were now embedded within the bondline, so these regions of the panel were not used to produce single-lap joint specimens.

2.2.4 Shear lap testing

Uniaxial tensile loading of the specimens were performed in accordance with ASTM D5868-01 standard in a 100 kN capacity Instron load frame using displacement control at a crosshead displacement of 12.7 mm/min. Subsequently, failure load for each specimen was

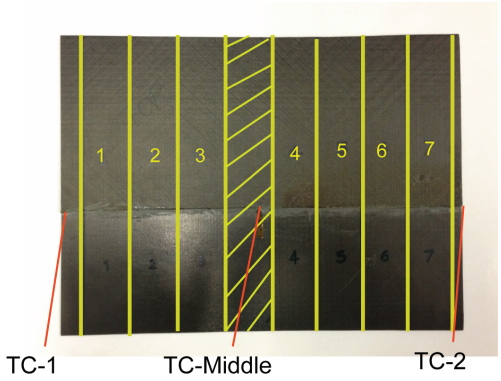

Figure 2.6: Photograph of cured single lap joint prior to cutting to shear lap specimens.

reported.

2.2.5 Cure analysis of SLJs using Differential Scanning Calilorimetry (DSC)

The cure of epoxy resins can be studied by DSC to give a quantitative measurement of the residual amount of reaction as well as determination of glass-rubber transition temperature (T_g). Furthermore, both quantities could be used to characterise the state of cure of a resin [42, 43]. Here, by testing an uncured sample the total energy that the cross-linking reactions required was calculated. subsequently, by testing the cured samples residual thermal energy that is needed for the material to be fully cured was measured using DSC Q2000 manufactured by TA Instruments.

2.2.6 Study of strain gradients in a bonded joint using Digital Image Correlation (DIC)

Experimental measurement of strains in the bond-line of an adhesively bonded joint can play a significant role in the design of bonded structures [44]; however, there are some difficulties associated in obtaining adhesive strains. One of the major difficulties is the small bond-line thickness. Therefore, non-contact optical methods are ideally suited for such measurements [45]. Digital Image Correlation (DIC) is a relatively new optical method that provides full-field displacements and strains while, being relatively simple in preparation and setup [46, 47]. Briefly, a speckled pattern is applied to the surface of interest, and a digital image

of the surface is recorded before and after loading. A correlation algorithm is then used to determine displacement fields caused by the loading. The displacement fields are then differentiated to obtain strains. Both two- and three-dimensional versions of DIC have been developed [48].

2.2.7 Shear strength results of single lap joints

Embedded carbon fiber fabric increases the effective stiffness as well as the thickness of the bondline. Consequently, specimens with and without embedded carbon fiber mesh were produced in an autoclave as well as in an oven to understand the potential effect of the embedded heater material on the overall performance of the bonded joint. As shown on Figure 2.7A, the oven cured joints without embedded fabric exhibited higher average shear lap strength, in comparison with similarly cured specimens with the embedded carbon fiber mesh. In contrast, autoclave cured samples with inclusion of the mesh had higher average strength comparing to the ones without the embedded fabric cured in similar condition. Nevertheless, shear lap testing results have shown that that the average joint performance where the adhesive was cured using embedded resistive heating was similar or higher than the other test samples regardless of their curing condition and inclusion/exclusion of the embedded fabric. Lap shear failure loads for bonded joints cured by embedded resistive heating, cured in oven and autoclaved are presented in Table 2.1. Figure 2.7B shows load vs. displacement curves for specimens close to the average strength of every curing method. Moreover, load vs. displacement curves were different with respect to curing method. Figure 2.8 shows typical failure surfaces for the samples with fabric embedded in the bondline cured through embedded resistive heating and autoclave. Failure for the electrically and thermally cured joints (autoclave and oven cured samples) was observed to be a combination of interfacial failure and cohesive failure of the adhesive. Moreover, failure for the two specimen types was very similar and occurred partially close to the adhesive and composite inter-face, and partially between the uni-directional fabric and the adhesive. Some carbon fibers were also pulled out from the adherend surface. The failure surfaces were consistent with the similar joint strengths measured for the thermally and electrically cured samples

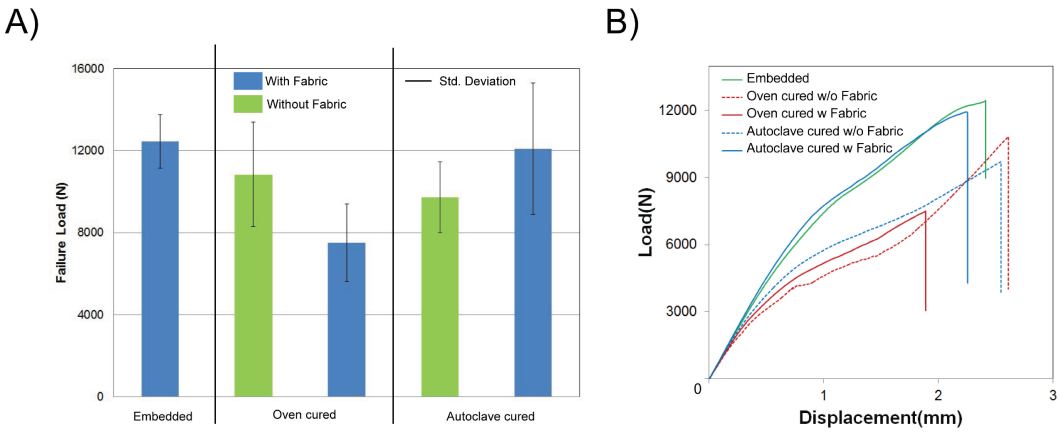

Figure 2.7: A)Average lap shear faiilure loads for the single lap joints. B)Load vs. displacement curves for specimens closest to the average strength of every curing method.

(Table 2.1).

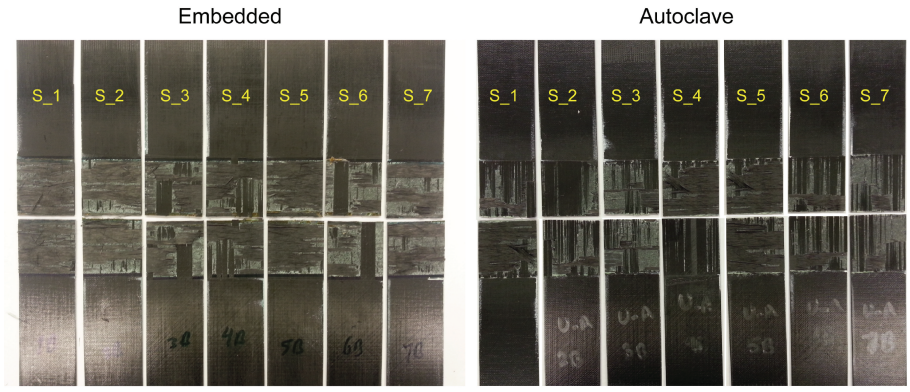

Figure 2.8: Failure surfaces of the single lap joints with inclusion of mesh fabric.

2.2.8 Cure analysis results by DSC

Three samples were chosen from each curing technique in a way to represent the lowest, closest to the average, and highest shear lap strength in each curing case. As shown on Figure 2.9 and in detail in Table 2.2 , cure analysis by DSC showed that samples cured by embedded heating method have comparable cure % with the ones cured in an autoclave.

No.	Embedded Fabric (N)	Oven Cured (N)		Autoclave Cured (N)	
		W/O Fabric	W Fabric	W/O Fabric	W Fabric
1	13997	8014	6676	11505	5605
2	13804	11058	4306	10630	11099
3	11708	13200	6401	8910	13064
4	10734	10898	8757	6359	14590
5	12737	14138	9161	9448	15288
6	11077	7118	8727	10251	11951
7	13177	11444	8543	10962	13096
Avg.	**12462**	**10839**	**7510**	**9723**	**12099**
Std. Dev.	1305	2540	1886	1726	3202

Table 2.1: Lap shear failure loads for all of the single lap test specimens.

Cure Method	No.	Failure Load (N)	Cure%
Embedded	1	13990	91.75
	4	10729	93.18
	5	12731	84.45
Oven	1	6672	95.06
	2	4306	70.91
	5	9159	97.06
Autoclave	1	5600	90.78
	5	15280	98.06
	6	11948	96.30

Table 2.2: Lap shear failure loads for all of the single lap test specimens.

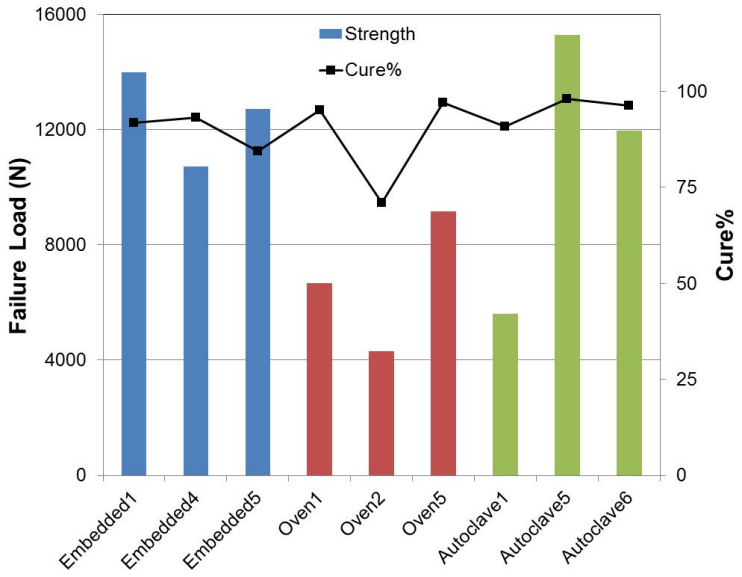

Figure 2.9: State of cure for selected samples vs. their shear lap strength.

2.2.9 Strain measurments results by DIC

Figure 2.10A shows maximum principal strain distribution results for five electrically cured bonded joints at 3336 N load level. Furthermore, maximum strain was observed on the edge as expected, and strain pattern was similar for all of the five test samples as well as the thermally cured specimens. As shown on Figure 2.10B, adhesively bonded joints that failed at higher loads showed higher joint stiffness than the rest of the samples. Although, the effect of joint stiffness on lap shear strength needs more investigation, this information could be potentially used to compare adhesively bonded joints strength by non-destructive shear lap tests in the future.

2.3 Conclusion

This chapter examined adhesively bonded single-lap joints where the adhesive was cured using heat generated by passing an electrical current through a carbon fiber fabric embedded in the bondline. It was shown that joints cured by embedded resistive heating method can provide equivalent shear strength to oven- and autoclave-cured joints. These results

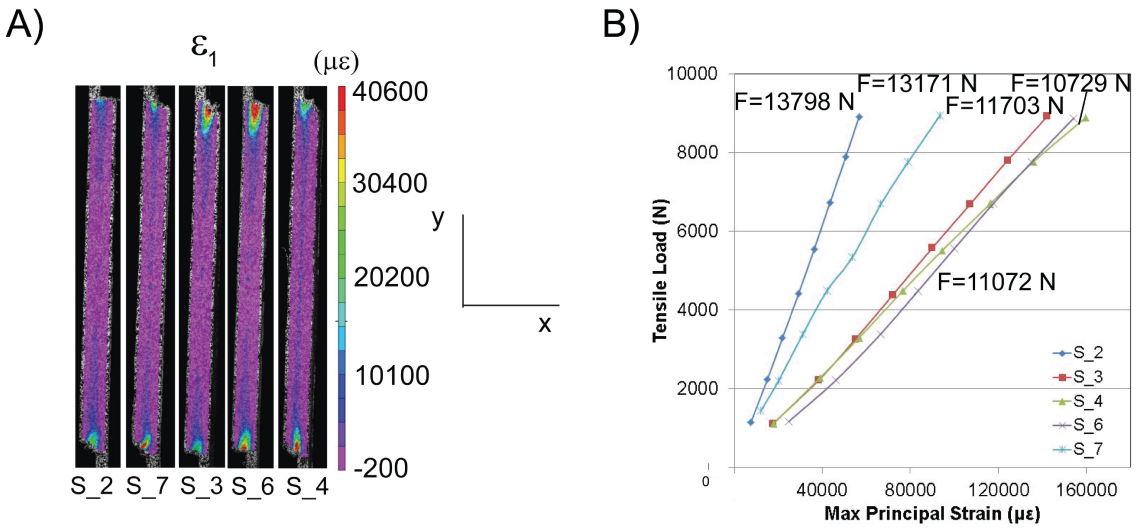

Figure 2.10: A) Maximum principal strain for samples cured by embedded resistive heating method. B) Maximum principal strain for samples cured by embedded resistive heating method.

indicate that this technique is capable to adapt to typical repair configurations with complex geometries and adhesives with different physical and chemical properties. Additionally, strain measurements using DIC showed that bonded joints with higher failure loads indicated higher joint stiffness in comparison with other test samples. It was shown rather than heating the entire system to cure the adhesive, controlled heating using an embedded carbon-fiber fabric was targeted at the bond-line. By localizing the heating to where it is needed, the proposed approach can substantially reduce the energy and cost of joining composite components, when compared to the use of autoclaves.

Chapter 3

RESISTIVE EMBEDDED HEATING IN COMPOSITE SCARF REPAIRS

In the previous chapter, embedded resistive heating was used to cure adhesives in single lap joints. To demonstrate the feasibility of the approach to real-world composite structural repairs, composite scarf repairs were cured using heat generated by passing an electrical current through a woven graphite-epoxy prepreg embedded in the bondline. Resistance heating using the embedded prepreg resulted in a more uniform temperature distribution in the bondline while preventing any potential thermal damage to the surface of the scarf repairs. Composite scarf repair specimens were created using the proposed embedded heating approach, and through the use of a heat blanket for circular and rectangular scarf configurations. Tensile tests were performed for rectangular scarf specimens, and it was shown that the bond strengths of all specimens were found to be comparable. The proposed embedded curing technique results in bond strengths that equal or exceed those achieved with external heating, and avoids overheating the surface of the scarf repairs.

3.1 History and Background

As more CFRPs are integrated into mportant applications such as transportation systems (aerospace, marine, and automotive), it has led to an escalation in maintenance/repair issues associated with composite materials [49, 50, 3, 51]. The primary objective of any structural composite repair technique is to restore the strength and stiffness of a damaged component and bring it to an acceptable service condition. Currently, the common techniques for repairing CFRP structures are: stepped co-bonded repairs, scarfed repairs, and bolted doubler repairs [3, 52]. In practice, scarf repairs are one of the most popular methods for repairing composite structures due to their convenience for execution, efficiency, and the reduction of stress concentrations at the bond length edges [50, 53, 54]. Yet, there are some challenges associated with scarf repairs as the thermal energy necessary to cure the

repair adhesive must diffuse through the composite layers to reach the joint repair interfaces, resulting in long and expensive processing times as well as wasted energy [5, 7, 8, 6]. Due to the shortcomings with the current repair practices, many deficient heating procedures have become standard practice even in approved aircraft repair manuals [4].

Here, it is proposed to overcome the mentioned difficulties by heating the bondline directly, instead of heating the entire structure. In the proposed heating method, electrical current passes through a woven graphite/epoxy prepreg sandwiched between two structural adhesive layers and in the bond serves as an embedded heater. Consequently, the heater will remain embedded in the bondline, contributing as a reinforcement agent. The embedded heater is made from the same material as the main structure, which could facilitate certification of the proposed approach for use in commercial aircraft.

In this chapter, an embedded resistive heating method for composite scarf repair was demonstrated for rectangular and circular scarf geometries. It is shown that this method achieved relatively uniform temperatures in the bondline avoiding possible overheating of the surface adjacent to the repair, which may occur when heat is applied using an external heater. The above targets where achieved without jeopardizing the structural performance of the repair.

3.2 Experimental Study

3.2.1 Materials

Flat laminates were produced using graphite/epoxy woven prepregs (Hexcel, BMS8-168) with $[0/+45/90/-45]_{2s}$ quasi-isotropic stacking sequence, and cured in an autoclave according to the curing cycle suggested by the prepreg manufacturer (3 °C/min heat-up rate, 130 min hold at 128 °C with 586 kPa external pressure with vacuum). The composite laminates were then cut to 30.48 cm × 15.24 cm plates using an abrasive disc. The graphite/epoxy woven prepreg used in the laminates was also used as the embedded resistive heater, and is shown on Figure 3.1A. The prepreg was cut to the dimensions (279.5mm × 152.4mm) depicted in Figure 3.1B. Two layers of 1.27 cm wide copper tape were attached to the embedded heater to evenly distribute the applied electrical current. Additionally, the

embedded heater was designed to be wider than the repair area to reduce potential edge effects. Two layers of structural adhesive film (3MTM Scotch-WeldTM AF163-2K) with nominal 0.254 mm thickness were used to bond the adherends. Modulus of elasticity, shear modulus, and Poisson's ratio of the structural adhesive were reported by its manufacturer to be 1110 MPa, 414 MPa, and 0.34 at 24 °C respectively.

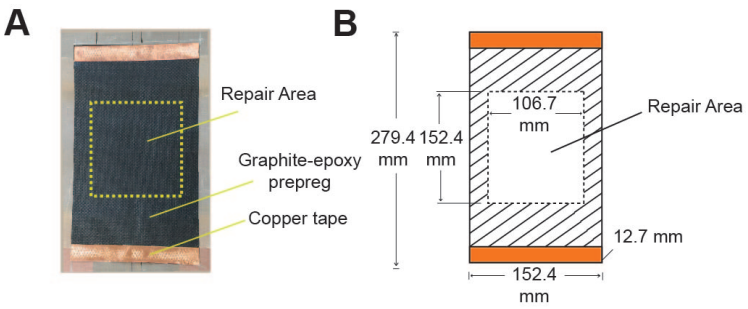

Figure 3.1: A) Graphite-epoxy prepreg used as the embedded resistive heater. B) Schematic of the embedded graphite-epoxy prepreg.

3.2.2 Repair design

In this chapter, scarf repairs were completed for two different scarf configurations (rectangular and circular geometries) in order to show the feasibility of the embedded resistive heating process. Furthermore, the circular scarf configuration represents the typical scarf composite repair geometry while the rectangular scarf configuration was chosen to facilitate producing similar tensile specimens to evaluate the repair. The scarf configuration corresponds to a repair procedure where a laminate is deemed to have suffered damage at an intermediate section. Then, the damaged region is removed by grinding the damaged material, resulting in a scarf shape. In practice material is often removed using a hand-held grinder, but during this study material was removed using a Computer Numerical Control (CNC) machine to insure a well-defined geometry. A scarf angle on the order of 5° is used for all composite repairs, regardless of stacking sequence following the study by reference [54] for similar stacking sequence. Figure 3.2A shows the geometrical details of the scarfed plates. Similarly, pre-cured plugs with the complementary shape of the removed material

were also created using a CNC machine. The geometry of the pre-cured plugs is presented in Figure 3.2B. It should be noted that pre-cured plugs were produced for two different thicknesses (h). Firstly, a pre-cured plug for the conventional external heating method, h=4.32 mm. Secondly, a pre-cured plug for the embedded resistive heating method, h=3.94 mm. This difference was designed to account for the added thickness in the bondline caused by the addition of the embedded heater.

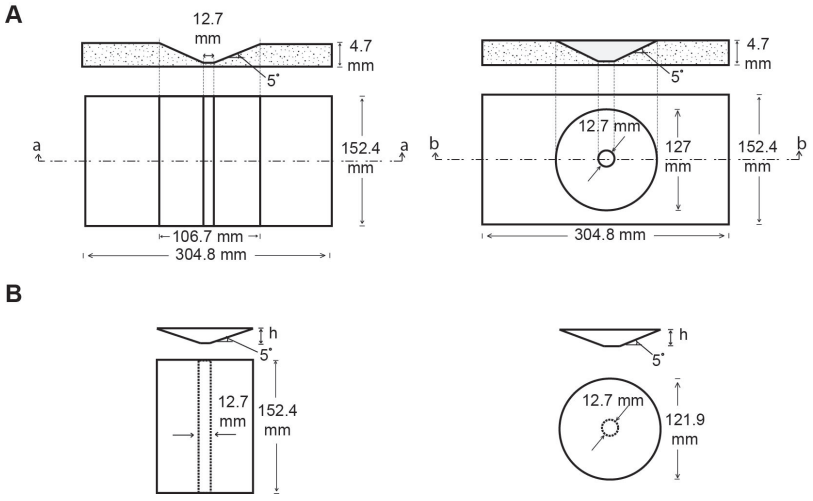

Figure 3.2: A) Schematic of the rectangular and circular scarfed plates. B) Schematic of the pre-cured plugs for the rectangular and circular scarfed plates.

3.2.3 Embedded resistive curing of scarf repairs

Carbon/epoxy composite panels are electrically conductive, and might interfere in the resistive heating process in the case of any contact between the embedded fabric and adherends. The adhesive films were cut slightly larger than the repair area to ensure that there was no contact between the embedded fabric and the adherends. Resistance testing was conducted to ensure complete electrical insulation between the embedded fabric and the composite parts, prior to the experiments. In the bond region, a layer of structural thin adhesive film was placed on each side of woven graphite/epoxy prepreg. Figure 3.3A shows a cross-sectional schematic of the embedded resistive repair of a rectangular scarf repair. A 1.27

cm thick silicon rubber sheet was used to thermally insulate the experimental system from the bottom. Covering each experiment was several layers of polyester breather fabric to minimize the heat transfer from the top section. All of this was covered with a vacuum bag, as shown on Figure 3.3B. Consequently, vacuum pressure was applied to the setup prior to the heating process, and was kept at 33.86 kPa until the sample reached the ambient temperature. Figure 3.4A shows the experimental setup prior to insulation and vacuum bagging. The end-to-end resistance of the woven prepreg was measured to be 1.5 Ω, and therefore the maximum power generated was approximately 83 W which is considerably lower than the 180 W generated from the heat blanket used in this study. The power supply was connected in series with a solid state relay (SSR), and the average value of the K-type control thermocouples feedback, was used to control temperature during the curing process using an Arduino Mega microcontroller board. The temperature increase rate was 3 °C/min, followed by maintaining the control temperature at 127 °C for 90 mins, and then the repair area was allowed to cool not faster than 3 °C/min.

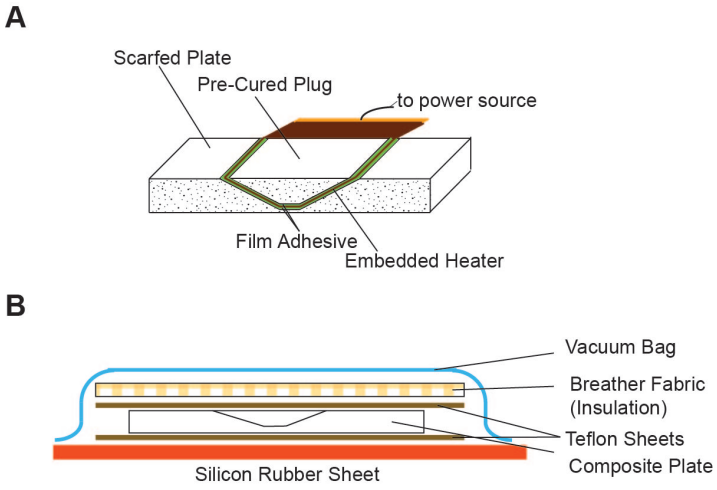

Figure 3.3: A) Schematic of the experimental setup for embedded resistive curing of a rectangular scarf repair. B) Schematic of the materials surrounding the repair.

3.2.4 Curing scarf repairs using an external heat source

In this study, external heating using a heat blanket was compared to the embedded resistive heating of composite scarf repairs. In-bond temperatures as well as tensile strength of the repaired specimens were evaluated. A 15.24 cm square Silicon rubber heat blanket (Heatcon® HC060060E51), rated for 120 V and 180 W, sitting on top of a Teflon sheet was used to heat the repair adhesive. Additionally, a system identical to the embedded resistive heating method was used to control the repair process. Figure 3.4B shows the experimental setup prior to and after insulation and vacuum bagging.

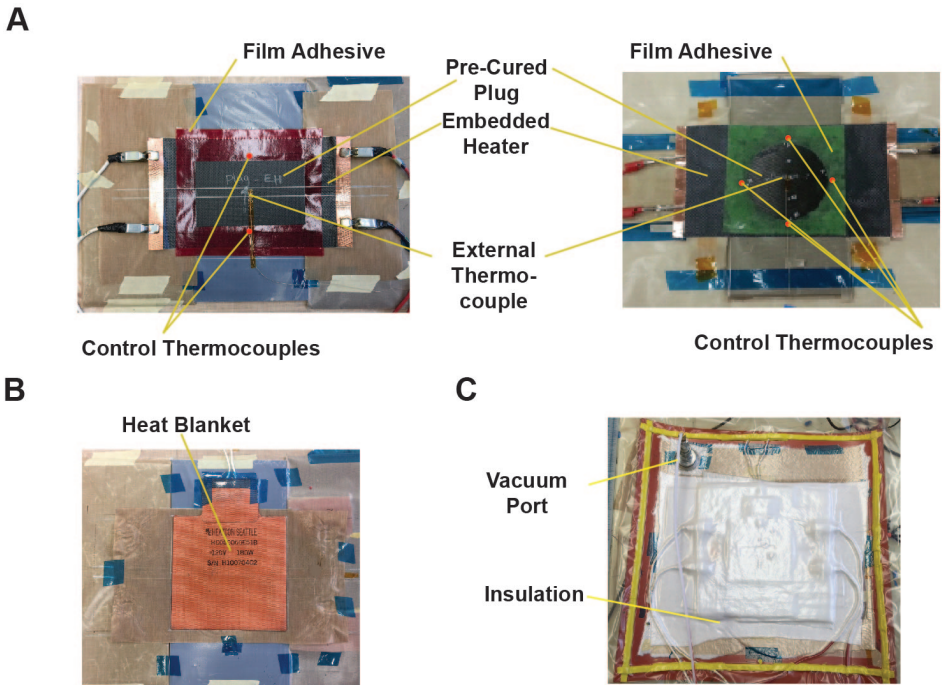

Figure 3.4: A) Photograph of the experimental setup prior to vacuum bagging and insulation for rectangular and circular scarf repairs. B) Photograph of the heat blanket used for external heating of the scarf repairs. C) Photograph of the experimental setup after vacuum bagging and insulation.

3.2.5 Temperature measurement in the repair area

In this study, an empirical approach (dry-run) was used to measure the temperatures inside the bond-line prior to the repair process. In the dry-run stage, the structural-film adhesive used during joining is replaced with (non-adhesive) Teflon electrically insulating sheets to prevent adhesive bonding, and electrical shorting. A total number of 15 sensors were used to record the temperatures, as shown on Figure 3.5. For the rectangular scarf repairs, the temperature sensors were embedded in a 106.7 mm × 106.7 mm area (test area) to comply with the square shape of the external heater. Moreover, the samples used for structural testing were machined from this test area.

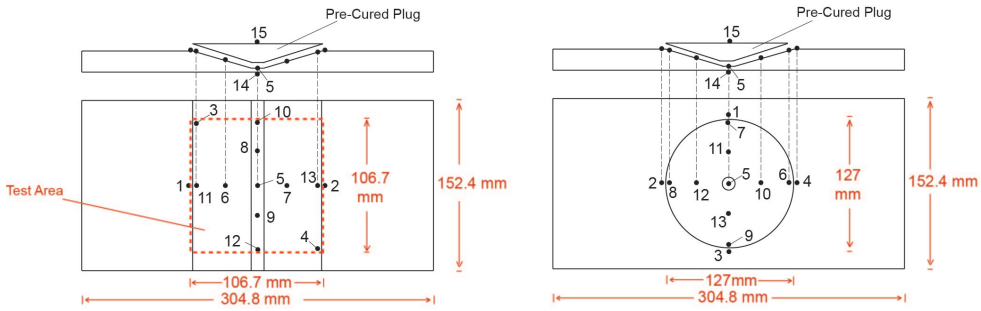

Figure 3.5: Schematic of the scarf repairs showing the location of the thermocouples in the dry-runs.

3.2.6 Temperature uniformity in the repair area

Structural film adhesives are typically cross-linking thermosets (e.g., epoxies) and require precise control of the temperature profile (both spatial and temporal) to cure properly. Thus, temperature uniformity in the bond-line is a matter of great importance in composite repairs. Figure 3.6 shows the temperature data feedback recorded by all eleven thermocouples embedded in the bond-line for the resistive heating method during the dry-run stage. Temperature contour plots were plotted at the 100^{th} minute after the start of experiments by interpolating the point-by-point readings between the embedded thermocouples.

In the rectangular scarf samples cured via embedded resistive heating a significant temperature gradient was observed to be perpendicular to the current flow due to the edge

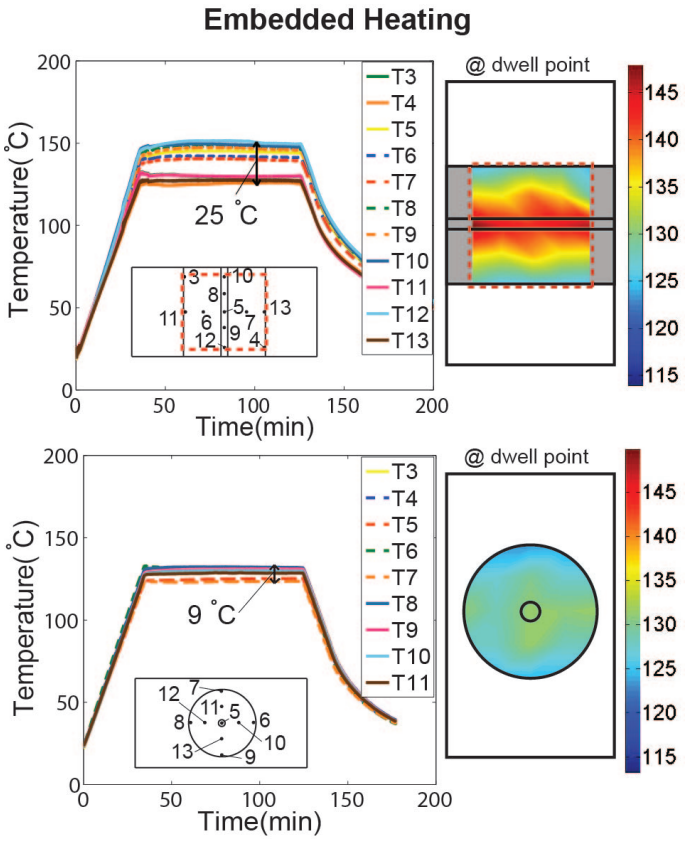

Figure 3.6: Temperature recordings from the thermocouples inside the bond area for rectangular and scarf repairs in the embedded resistive heating method.

effect. Yet, this effect was not apparent in the circular scarf dry-run due to a better insulation by the circular pre-cured plug. Figure 3.7 presents the temperature data feedback recorded by the embedded in the bond for the external heating method in the dry-run stage. The measured in-bond temperature gradients were 30% and 59% higher at the dwell point (where the temperatures are held constant over an extended period of time) for the rectangular and circular scarfs respectively with the external heating method.

3.2.7 Surface temperature in composite scarf repairs

In practice, heat flux needs to pass a couple of layers of fabrics in addition to the repair material in order to reach to the bond area. This results in through thickness thermal gradi-

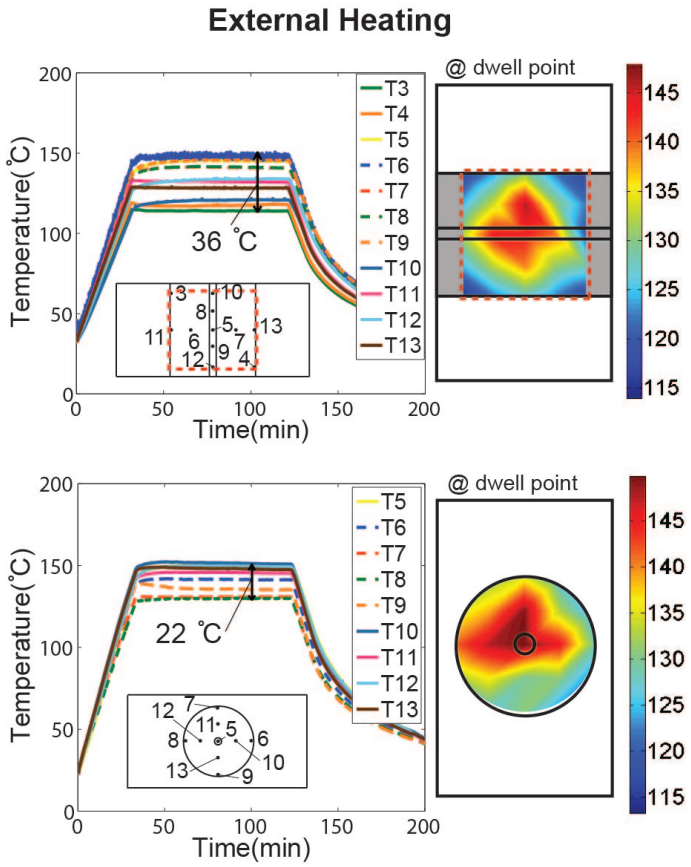

Figure 3.7: Temperature recordings from the thermocouples inside the bond area for rectangular and scarf repairs in external heating method.

ents, which leads to over-heating the surface of the repair material adjacent to the external heater. Unfortunately, surface over-heating is inevitable, and many deficient heating procedures have become standard practice even in approved aircraft repair manuals [4]. In this paper, through thickness temperature gradient for the repairs by resistive heating method was measured at 3 points, and is shown on Figure 3.8A. The highest measured temperature in the mentioned method was recorded in the bond area, while the lowest values were recorded in the outer repair surface. Therefore, the embedded resistive heating method delivers the heat flux to the location that it is required, i.e., in the bondline. Figure 3.8B shows the temperature feedback from the thermocouples embedded through the thickness of the repaired plate for the external heating process. The highest temperature values were

recorded at the thermocouples located on the surface of the repair as expected. Additionally, surface temperatures in external heating were 11% and 27% higher than resistive heating in rectangular and circular scarf repairs respectively.

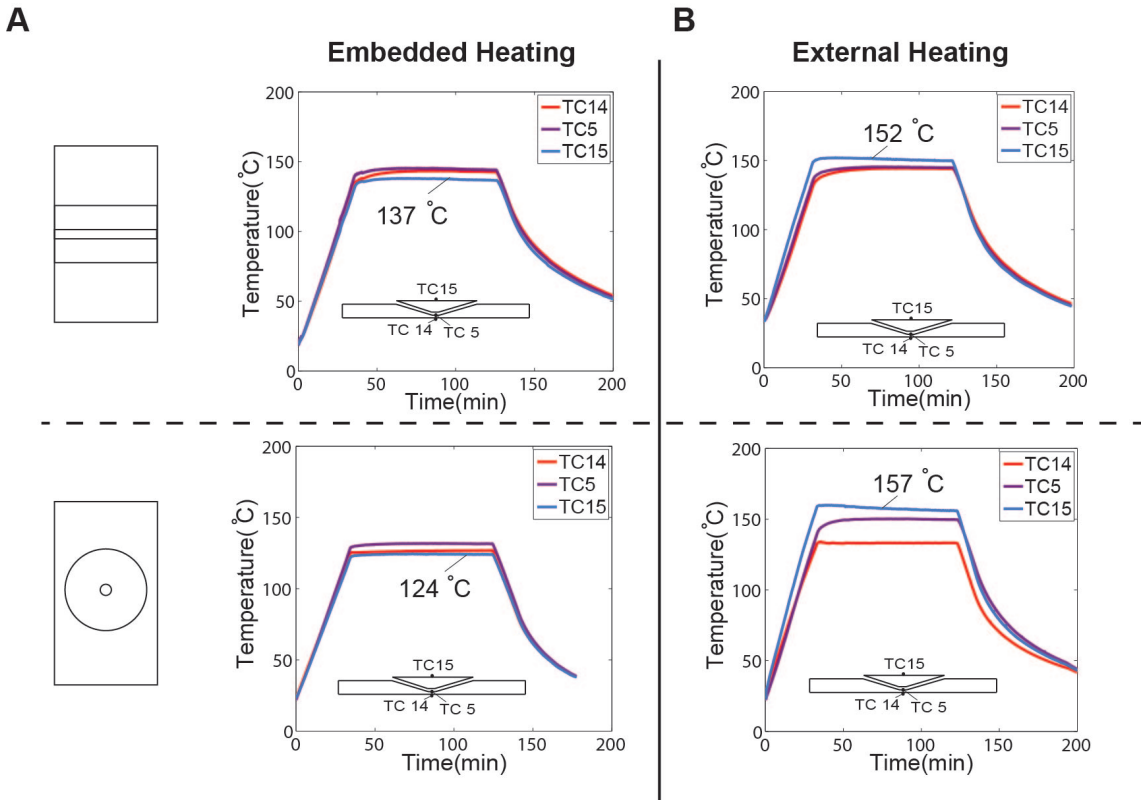

Figure 3.8: A) Temperature feedback from the thermocouples located through the thickness of the rectangular and scarf repairs in the embedded resistive heating method. B) Temperature feedback from the thermocouples located through the thickness of the rectangular and scarf repairs in the external heating method.

3.2.8 Tensile strength of scarf repair joints

Four scarf specimens were produced from the test area in each of the two square scarf panels, resulting in a total number of 8 tensile specimens with 25.4 mm thickness were tested for each repair method. Uniaxial tensile loading of the specimens was performed by a 100 kN capacity Instron load frame using displacement control at a crosshead displacement of 12.7

mm/min. Subsequently, failure load for each specimen was reported. The embedded carbon fabric increases the effective stiffness as well as the thickness of the bond-line, however, no significant difference in structural performance was observed in our previous studies due to this effect [5, 39]. As shown in Figure 3.9A, scarf repairs cured through embedded resistive heating exhibited slightly higher average tensile strength, in comparison with specimens cured using external heating method. Figure 3.9B shows load vs. displacement curves for specimens close to the average strength of both curing methods. Moreover, no significant change in stiffness was observed between the two techniques. The variance in the tensile testing data for the external heating method was higher than results with the embedded resistive heating experiments, which could be indicative of a small sample size. Fracture in all samples started in the top layer of the repair plugs, followed in the bond-line, and finally it reached the bottom layers of the laminates, as shown on Figure 3.10A. Figure 3.10B shows typical failure surfaces for the samples cured through embedded resistive heating and external heating techniques. Failure for all of the specimens was observed to be a combination of interfacial failure and cohesive failure of the adhesive. Moreover, failure for the resistive heating samples was very similar and occurred partially close to the adhesive and composite inter-face, and partially between the embedded prepreg fabric and the adhesive. Whereas, failure happened close to the adhesive and composite inter-face for the external heating specimens. The similarity between the failure modes is consistent with the comparable average tensile testing results.

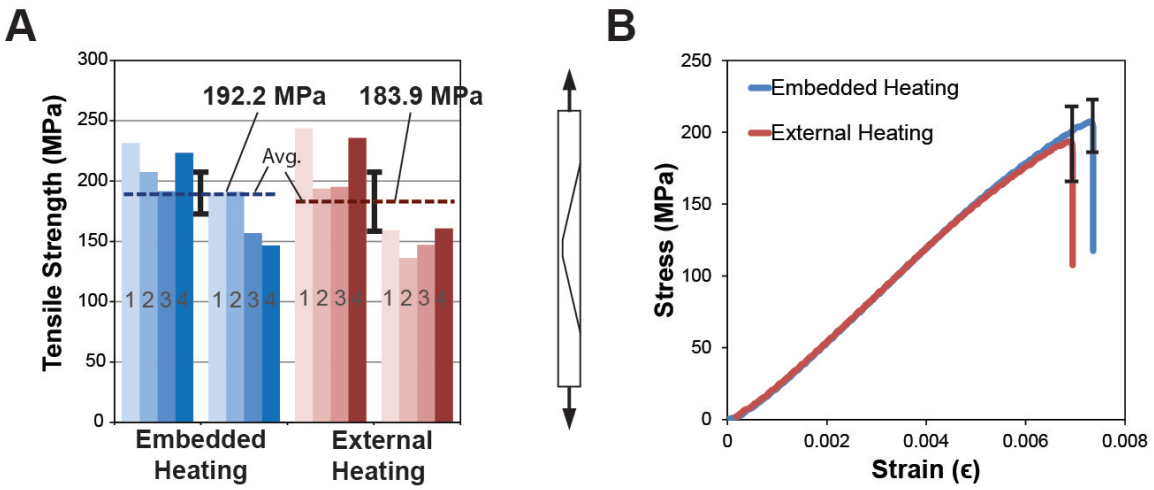

Figure 3.9: A) Tensile strength of the rectangular scarf specimens. B) Typical Stress vs. strain curves for specimens cured using embedded heating and external heating methods.

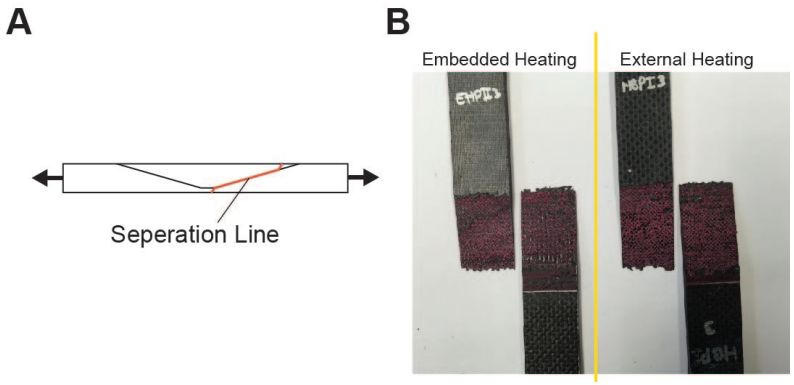

Figure 3.10: A) Schematic of the failure mode for a typical rectangular scarf test specimen in both repair methods. B) Failure surface of a typical tensile specimen from both repair methods.

3.3 Conclusion

This study examined composite scarf repairs where the adhesive was cured using heat generated by passing an electrical current through a woven graphite/epoxy prepreg fabric embedded in the bond-line. It was shown that rather than heating the entire system to cure the adhesive, controlled heating using an embedded carbon-fiber fabric can be used to target temperature increases at the bond-line. By localizing the heating to where it is needed, the proposed approach can reduce the energy and cost of repairing composite components, when compared to the use of heat blankets. Moreover, embedded resistive heating provides lower in-bond temperature gradients in the scarf repairs, and can avoid surface thermal damage that may occur with the external heating method. Additionally, repairs cured by embedded resistive heating method provided average tensile strengths at least as high as samples cured via external heating method. These results indicate that this technique is capable to adapt to typical repair configurations with complex geometries and adhesives with different physical and chemical properties.

Chapter 4

THERMAL-ELECTRIC FINITE ELEMENT MODEL OF THE EMBEDDED RESISTIVE HEATERS

In every bonding/repair application, the amount of heat flux needed to cure the bond varies based on material type, thickness and surrounding structures. In this Chapter, two-dimensional and three-dimensional thermoelectrical finite element models of embedded resistive heaters with different geometries and boundary conditions were performed using the commercial finite element package ANSYS. The predicted temperatures through Finite Element Method (FEM) could be used to design specialized embedded resistive heaters that could potentially reduce the thermal gradients caused by the presence of heatsinks, and thereby decrease or eliminate the time and cost associated with designing embedded heaters.

4.1 History and Background

The Finite Element Method (FEM) has become an essential tool in engineering applications due to its ability to model arbitrary shaped structures, work with complex materials, and apply various types of loading and boundary conditions. The ANSYS finite element program has a large library of elements that support structural, thermal, fluid, acoustic, and electromagnetic analyses, as well as coupled-field elements that simulate the interaction between the above fields [55]. Coupled thermal-electric finite element modelling provides a powerful tool to predict the induced temperatures in an structure when passing an electrical current. Moreover, researchers have used FE modelling to predict thermal damages induced in composite structures due to lightning strike [56, 57, 58]. Thermal-electric FEM has also proven to be an effective tool in understanding the Resistance Spot Welding (RSW) process in quantitative details [59, 60, 61]. In particular, Cho and Cho [62] predicted the temperature and voltage distribution incorporating the thermoelectric interaction at the interface in the weldment. In a composite structure system, surrounding structures (e.g.,

stringers or frames) often act as heat sinks, generally increasing both through-thickness and in-plane thermal gradients. Here, FEM was used to account for the Joule heat as a coupling mechanism between thermal and electric fields.

The temperature difference induced in a resistive heater by applying electrical voltage from single or multiple sources was investigated in this Chapter. Similar conductors (copper) have been used in the experiments, and therefore, thermoelectric effects such as Seebeck's, Thompson's, and Peltier's effects were neglected in this study. Thus, Joule heat is considered as the only coupling mechanism between the thermal and electric fields. A major objective in a conduction analysis is to determine the temperature field in a medium resulting from conditions imposed on its boundaries. The steady state finite element model computes the temperature and voltage distribution in the elements as a function of spatial co-ordinates. The thrmal and electrical governing equations are independent of time in the steady state finite element model. The governing heat diffusion equation and boundary conditions for our system is described in Appendix C.

4.2 Two-Dimensional FE model for temperature distribution

Two-dimensional FE models are simple to prepare and execute. Moreover, in the studied embedded resistive heaters had relatively small thicknesses in the normal direction, and hence the temperature difference in the normal direction is minimal.

4.2.1 Geometry and meshing

Here, a circular embedded resistive heater was modeled in ANSYS 15.0 in a steady state analysis. A single input system (Figure 4.1A) refers to a system where a potential difference of 5 V is applied to one edge of the embedded heater, while another edge is attached to the ground. Additionally, when two edges of the heater are subjected to 5 V of electrical potential, and two edges are attached to the ground it will benoted as a double input system (Figure 4.1B). The geometry was then meshed using four node elements. Finer meshing scheme was used at the edges where the electrical potential difference were applied. The resulting elements are shown on Figure 4.1C and Figure 4.1D.

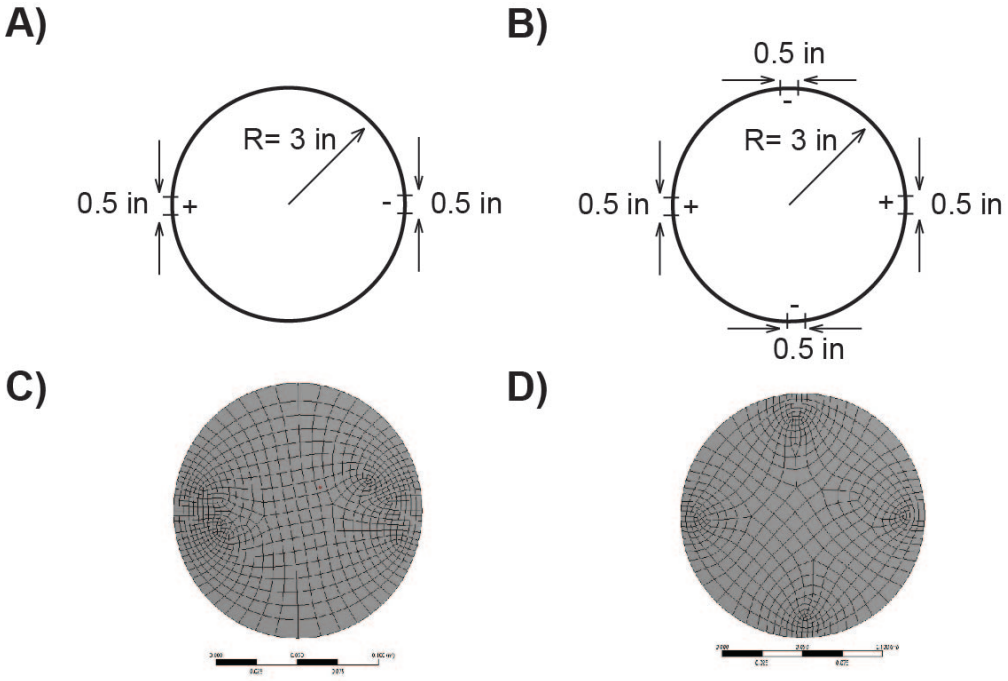

Figure 4.1: A) Schematic of the circular resistive heater in a single input system. B) Schematic of the circular resistive heater in a double input system. C)Finite Element mesh of the single input system. D)Finite Element mesh of the double input system.

4.2.2 Material properties used in the two-dimensional model

Resistive heaters that were modeled in this study are from the same material described in Chapter 3. Heater's electrical resistances for different widths, and a constant length and thickness of 11 in and 0.1 in respectively, were measured using a resistance meter, and the results are plotted in Figure 4.2. Note that the resistance meter's resolution was $\pm 2.5\Omega$, and therefore the measured resistance did not seem to reduce with the increase in width in the last 3 data points. Low-resistance measurements are subject to many of the same sources of error as low-voltage measurements, including offset voltages due to thermoelectric Electric and Magnetic Fields (EMFs), offsets generated by rectification of radio frequency interference (RFI), and offsets in the chosen instruments voltmeter input circuit. Noise sources that can interfere with low-resistance measurement accuracy include Johnson noise, magnetic fields, and ground loops [63]. Thermal conductivity coefficients used in this study

were measured by reference [64] to be $6.21\frac{W}{m.K}$.

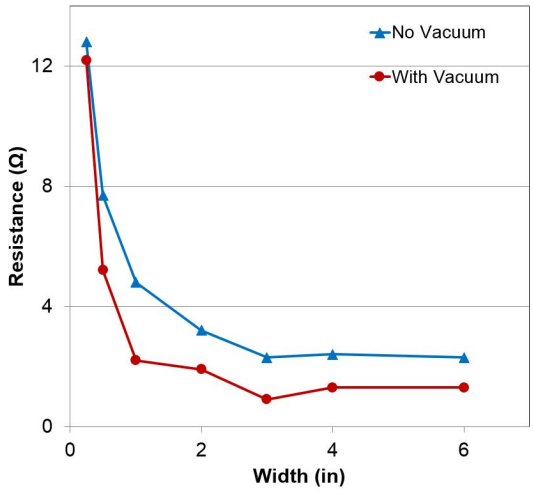

Figure 4.2: Measured electrical resistance of resistive heaters with and without pulling a vacuum

4.2.3 Results and discussion

The steady state temperature distribution obtained using ANSYS for a single input system is shown on Figure 4.3A, and was compared to experimental measurements using a thermal camera presented on Figure 4.3B . Although the FE model tends to predict the temperature distribution across the repair area relatively well, the temperature values were found to be significantly higher than the experimental measurements. Similarly, the steady state temperature distribution obtained using ANSYS for a double input system is shown on Figure 4.4A, and was compared to experimental measurements using a thermal camera presented in Figure 4.4B. In this two-dimensional FE study, the out of plane convection was assumed to be negligible, which led to discrepencies between FE predictions and experimental temperature measurement.

4.3 Three-Dimensional FE model for temperature distribution

Following the discussion in the previous section, a three-dimensional finite element model was prepared to account for the heat loss through out-of-plane thermal convection.

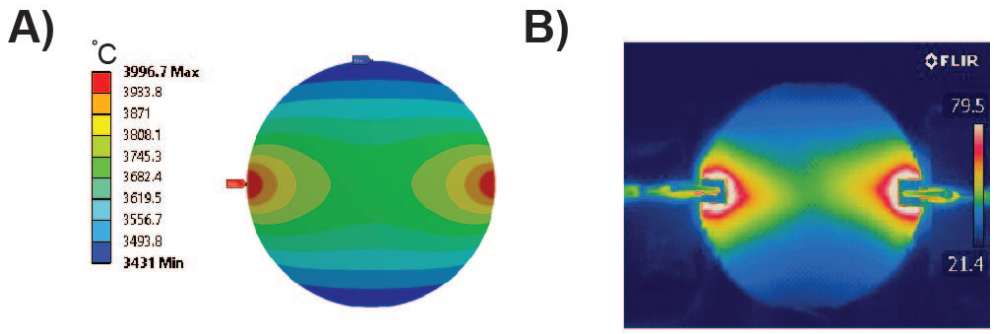

Figure 4.3: Steady state temperature distribution through A) FE modeling B)Thermal Camera

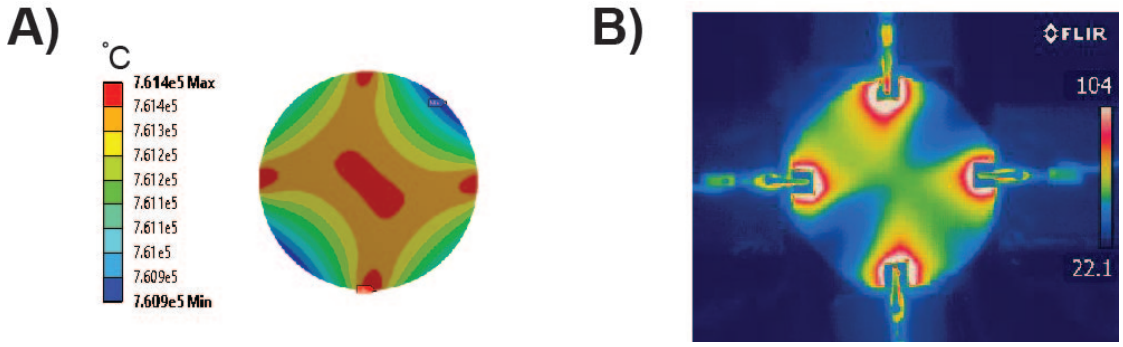

Figure 4.4: Steady state temperature distribution through A) FE modeling B)Thermal Camera

4.3.1 Geometry and meshing

A $15.24cm \times 15.24cm$ square shaped heater with the thickness of 0.279 mm was designed in the FE software to be similar to the embedded heater chosen for the experiment shown on Figure 4.5A. Square slots with the size of $1.27cm \times 1.27cm$ were cut on every side to represent the copper tapes planted on the embedded heater. Figure 4.5B presents a schematic for the FE model used in this study. The resulting model was then meshed using four node elements. In this study, a similar meshing scheme was used in accordance to the two-dimensional models.

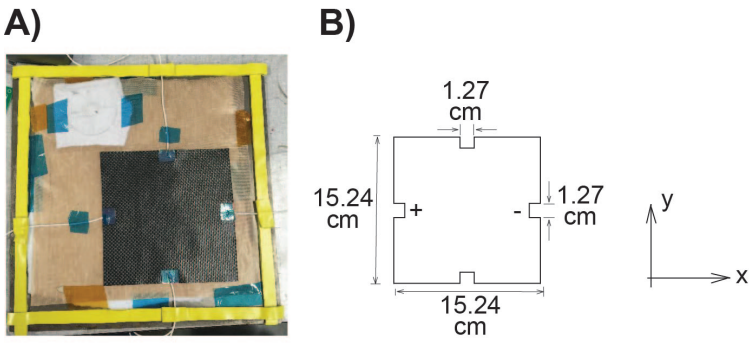

Figure 4.5: A) Graphite-epoxy prepreg used as the embedded resistive heater. B) Schematic of the modeled embedded graphite-epoxy prepreg.

4.3.2 Material properties and boundary conditions

Vacuum pressure presses the conductive graphite fibers together, and therefore significantly changes the electrical resistance of the embedded heater. Therefore, the resistivity of the heater was evaluated in 10 mmHg and kept constant while passing electrical current from the heater. The resistivity of the embedded heater was evaluated to be 0.1082 $\Omega.cm$ and 0.0932 $\Omega.cm$ in x and y directions respectively. Thermal conductivity coefficients (k_x and k_y) were assumed to have the same linear relation as the resistivity to be $21.4\frac{W}{m.K}$ and $25\frac{W}{m.K}$. One face of the heater was defined to be perfectly insulated while the opposite face of the embedded heater was assumed to lose heat through convection with $55\frac{W}{m^2{}^\circ C}$ in thermal convection coefficient. Finally, 10 V of electrical potential difference was applied to the heater's $1.27cm$ edges.

4.3.3 Verification

The steady state temperature distribution obtained using ANSYS for a single input system is shown on Figure 4.6A, and was compared to experimental measurements using a thermal camera presented on Figure 4.6B. Furthermore, the steady stae temperature distribution model was in good agreement with the experimental measurement.

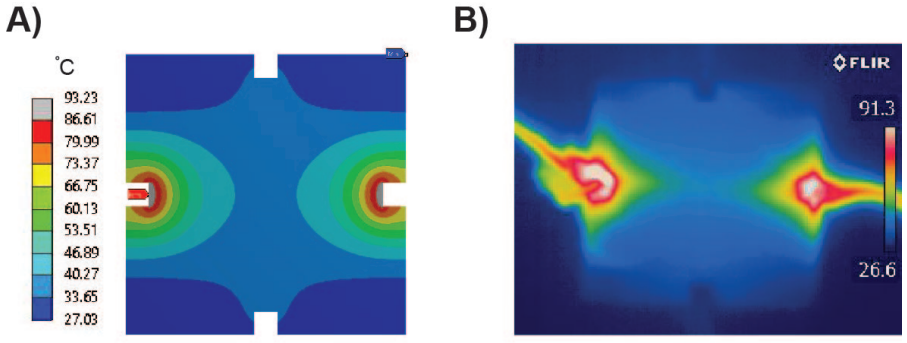

Figure 4.6: Steady state temperature distribution through A) FE modeling B)Thermal camera

4.3.4 FE model of embedded heaters with more than one input

The heat distribution on the embedded heater changes as the boundary values ν of the potential V is modified at the externally accessible edges of the heater. This could be particularly beneficial to address the potential heat sinks in a composite repair by targetting the heat to a zone with higher amount of heat loss. To further explain and verify this concept, a double input and a triple input square models were compared to the single input heater that was described in the previous section. Schematic of the FE models are presented in Figure 4.7.

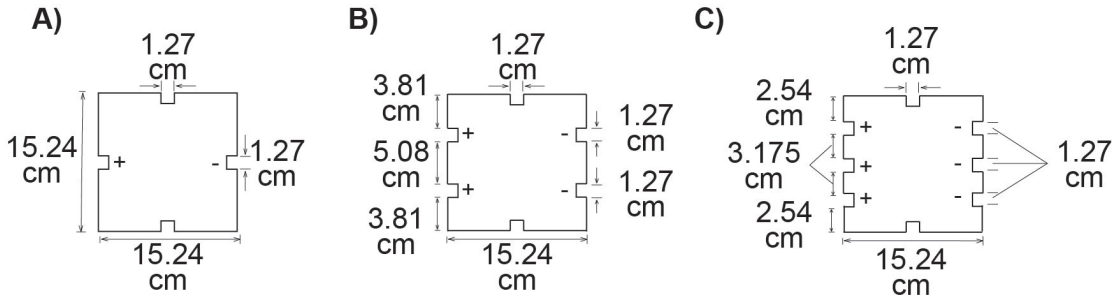

Figure 4.7: Schematic of the modeled embedded heater in A) single input B)double input C) triple input system

Material properties and boundary conditions used in this study were identical to the ones used in section 4.3.2. Figure 4.8 shows the electrical potential and temperature distribution

in all three models. Furthermore, in the single-input model the temperature gradient across the heater was predicted to be 66.2 °C. As the electrical potential became more evenly distributed in the edges in the double input and triple input systems, the temperature gradients were decreased by 41.5% and 61.1% respectively.

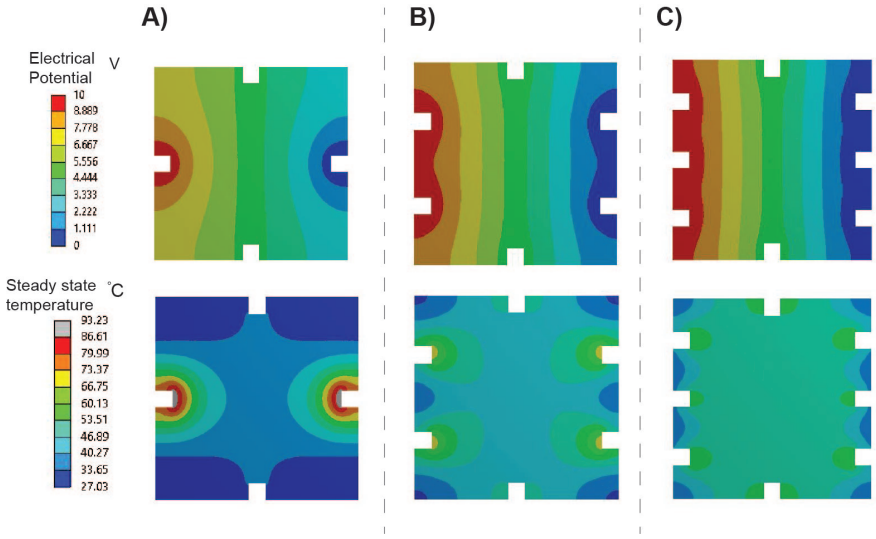

Figure 4.8: Steady state electrical potential and temperature distribution in A) single-input B)double input C) triple input system

4.3.5 Addressing potential heatsinks by modifying the boundary values

In the previous section, it was shown that the heat distribution on a heater could be changed when the boundary values of the potential V is modified. This feature could be used in this section to address potential heatsinks present around a bonding area.

To show this concept, an embedded heater was modeled with three heat zones, as shown in Figure 4.9.

Here, the presence of a heatsink was modeled through modifying the value of the thermal convection coefficient. Three different boundary conditions used to study the effect of a heatsink applied to zone II in Figure 4.9. Case A presents an embedded heater with no heatsinks. Case B, shows a heater where the thermal coefficient of zone II was set to be 1.375 times of zone I and III. Finally, case C is when the heatsink was addressed by changing

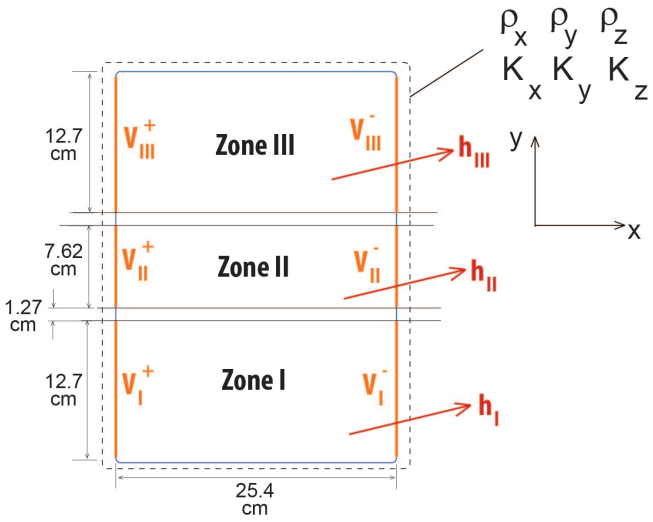

Figure 4.9: Schematic of the modeled embedded heater with three different heatzones

the applied electrical potential V_{II} to be 1.117 times of V_I and V_{III}. Figure 4.10 shows the steady state distribution of the temperature in all three cases. Furthermore, FE results show that the boundary values could be optimized to address potential heatsinks. By changing the boundary values, the in-bond thermal gradients were decreased by 78% .

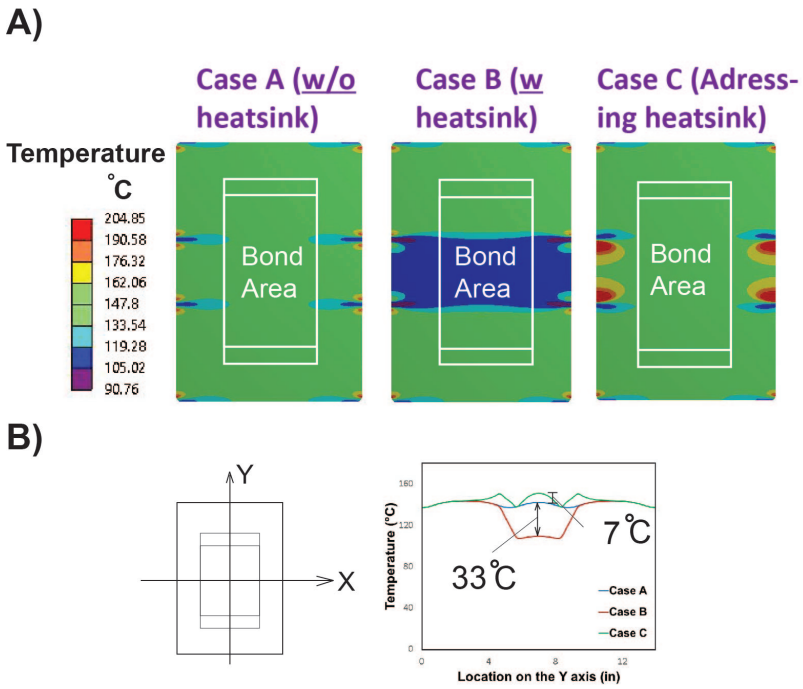

Figure 4.10: A)Steady state temperature distribution in embedded heaters with three different boundary conditions. B))Steady state temperature distribution on the Y-axis in embedded heaters with three different boundary conditions.

4.4 Conclusion

Coupled thermal-electrical Finite Element program was used to predict the temperature distribution in an embedded heater as a result of applying an electrical potential. Three-dimensional FE models showed to have a good agreement with the pictures taken by a thermal camera from the experimental dry-run. Additionally, it was shown that by changing the boundary values of the electrical potential heat distribution on the embedded heater could be modified. Thus, The predicted temperatures through Finite Element Method (FEM) could be used to design specialized embedded resistive heaters that could potentially reduce the thermal gradients caused by the presence of heatsinks, and thereby decrease or eliminate the time and cost associated with designing embedded heaters.

Chapter 5

CONCLUSIONS AND FUTURE WORK

The research in this dissertation presented a an efficient adhesive-bonding approach for joining CFRP components in details. Rather than heating the entire system to cure the adhesive, it was cured using heat generated by passing an electrical current through a woven graphite/epoxy prepreg fabric embedded in the bond- line. This dissertation addressed three main issues: (i) adding a carbon-fiber fabric in the bond-line, (ii) repairing large areas, and (iii) maintaining uniform temperature in presence of heat-sinks/substructures.

It was shown that rather than heating the entire system to cure the adhesive, controlled heating using an embedded carbon-fiber fabric can be used to target temperature increases at the bond-line. By localizing the heating to where it is needed, the proposed approach can reduce the energy and cost of repairing composite components, when compared to the use of heat blankets. Moreover, embedded resistive heating provides lower in-bond temperature gradients in the scarf repairs, and can avoid surface thermal damage that may occur with the external heating method. Additionally, repairs cured by embedded resistive heating method provided average tensile strengths at least as high as samples cured via external heating method. These results indicate that this technique is capable to adapt to typical repair configurations with complex geometries and adhesives with different physical and chemical properties. Finally, the predicted temperatures through Finite Element Method (FEM) could be used to design specialized embedded resistive heaters that could potentially reduce the thermal gradients caused by the presence of heatsinks, and thereby decrease or eliminate the time and cost associated with designing embedded heaters.

In addition to the secondary-bonding applications, embedded resistive heating method could have an impact on manufacturing of composite structures by reducing the prohibitive cost of large autoclaves, and fabricating smaller parts and then joining them using this technique. Investigation on the feasibility of this approach in composite manufacturing could

be included in the future work.

Bonding technology in CFRP application could be classified into three main catagories [65, 66]:

1. Secondary-Bonding

   The joining together, by the process of adhesive bonding, two or more pre process of adhesive bonding, two or more pre-cured composite parts, during which the only cured composite parts, during which the only chemical or thermal reaction occurring is the curing chemical or thermal reaction occurring is the curing of the adhesive itself of the adhesive itself

2. Co-Bonding

   The curing together of two or more elements, of which at least one is fully cured and at least one is of which at least one is fully cured and at least one is uncured

3. Co-Curing

   The act of curing a composite laminate and simultaneously bonding it to some other uncured material, simultaneously bonding it to some other uncured material,or to a core material such as balsa, honeycomb, or foam or to a core material such as balsa, honeycomb, or foam core

Different bonding CRRP classifications are presented in Figure 5.1.

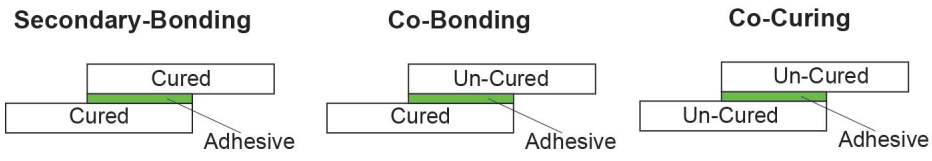

Figure 5.1: Classification of CFRP bonding methodologies

In this dissertation, embedded resistive heating method in secondary-bonding applications was studied in detail, and the results are presented in Chapters 2, 3, and 4. In a

secondary-bonding practice, the repair patch is already cured, and bonded to the damaged structure using a structural thin film adhesive. Embedded resistive heating applies the required heat flux needed for curing the thin film adhesive directly to the bond-line rather than heating it externally through the repair patch. Embedded resistive heating could also be combined with an external heating source to provide a uniform temperature accross the repair patch, when the repair patch is being cured during the repair (co-bonding) process. Schematic of the combined heating concept is depicted in Figure 5.2. Proof-of-concept, and some preliminary temperature measurements, and tensile testing data is included in Appendix D.

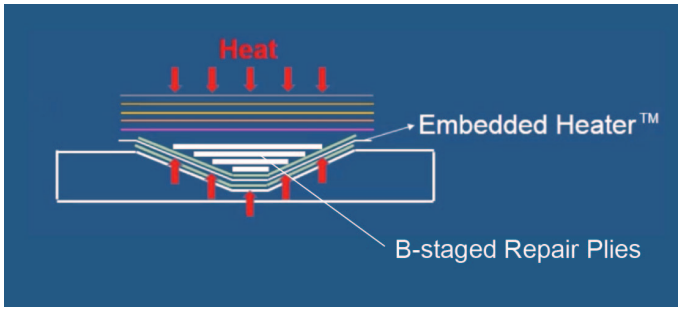

Figure 5.2: Schematic of Co-Bonding in composite repair by combining embedded resistive heating and external heating

Appendix A

GOLAND AND REISSNER CLOSED-FORM SOLUTION FOR SLJS

An important aspect of the optimal design process is formulation of the design problem in mathematical format which is acceptable to an optimization algorithm [67], and hence closed-form solutions play an important role in optimizing any mechanical design. In SLJs the stresses in the out of plane direction are significantly lower than in the direction of the loading, and therefore almost all analytical models for adhesively bonded lap joints are two-dimensional [68]. Adding carbon-fiber fabric in the bond-line increases bond-line stiffness as well as its thickness. Therefore, using a closed-form solution enables a quick evaluation of the potential changes on the stresses in the bond-line.

A.1 Obtaining governing equations for peeling and shear stresses in the bond-line by Goland & Reissner

Goland and Reissner [19] derived analytical Equations for peeling and shear stresses in the overlap of a SLJ by dividing the problem into two parts: (a) determination of the loads at the edge of the joint; (b) determination of the stresses in the joint due to the applied loads. A graphical presentation of the SLJ is shown on Figure A.1. Boundary conditions were applied, and the expressions of the following form are found for the moment and shearing force at the transition region between the adherend and the lap:

$$M_0 = \frac{Tt}{2} \frac{\sinh u_1 l \cosh u_2 c}{\frac{u_1}{u_2} \cosh u_1 l \sinh u_2 c + \sinh u_1 l \cosh u_2 c} \tag{A.1}$$

$$V_0 = \frac{Tt}{2} \frac{u_1 \cosh u_1 l \cosh u_2 c}{\frac{u_1}{u_2} \cosh u_1 l \sinh u_2 c + \sinh u_1 l \cosh u_2 c} \tag{A.2}$$

Where $u_1 = \sqrt{\frac{T}{D_1}}$ and $u_2 = \sqrt{\frac{T}{D_2}}$; D_1 and D_2 are flexural rigidity of the adherend and the bond respectively. The thickness of the adhesive (η) was assumed to be negligable in comparison with the adherend thickness (t), and therefore $D_2 \cong 8D_1$.

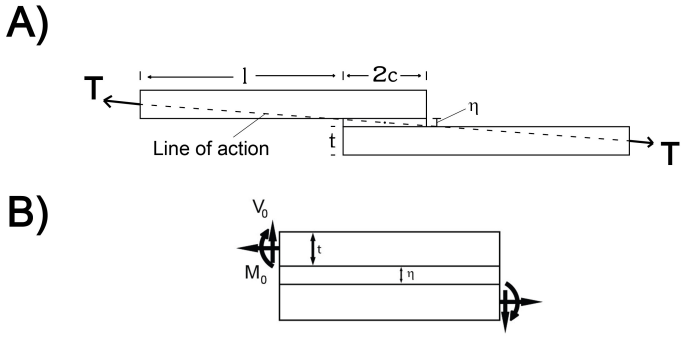

Figure A.1: A) Schematic of the specimen analyzed by Goalnd & Reissner . B) Diagram showing the loading applied on the joint.

In all practical cases the value of $u_1 l$ is large enough to assume $\sinh u_1 l \approx \cosh u_1 l \approx e^{u_1 l}$, and therefore Equation A.1 and A.2 can be reduced to:

$$M_0 = k\frac{Tt}{2} \tag{A.3}$$

$$V_0 = kT\sqrt{\frac{3T(1-\nu^2)}{Et}} \tag{A.4}$$

Where E and ν are the elastic moduli and Poisson's ratio of the adherend material respectively, and the value of k is dependant upon the applied load (T) and the phisyical properties of the adherend material in the following manner:

$$k = \frac{\cosh u_2 c}{\cosh u_2 c + 2\sqrt{2}\sinh u_2 c} \tag{A.5}$$

By analyzing the bond area, governing third and fourth order differential equations were derived for the shear (τ_o) and peeling (σ_o) stresses as follows:

$$\frac{\partial^3 \tau_o}{\partial x^3} = \frac{8G_c}{tE\eta}\frac{\partial \tau_o}{\partial x} \tag{A.6}$$

$$\frac{\partial^4 \sigma_o}{\partial x^4} = \frac{-24E_c(1-\nu^2)}{t^3 E\eta}\sigma_o \tag{A.7}$$

Where E_c and G_c are the elastic and shear modulus of the adhesive. After solving the governing differential equations and applying the boundary conditions found in the previous discussion, the distribution of shear stress is obtained in the following form:

$$\tau_o = \frac{-T}{8c}\left[\frac{\beta c}{t}(1+3k)\frac{\cosh\frac{\beta x}{t}}{\sinh\frac{\beta c}{l}} + 3(1-k)\right] \qquad \beta = \sqrt{\frac{8G_c t}{E\eta}} \tag{A.8}$$

A.2 Obtaining boundary conditions in Goland & Reissner solution

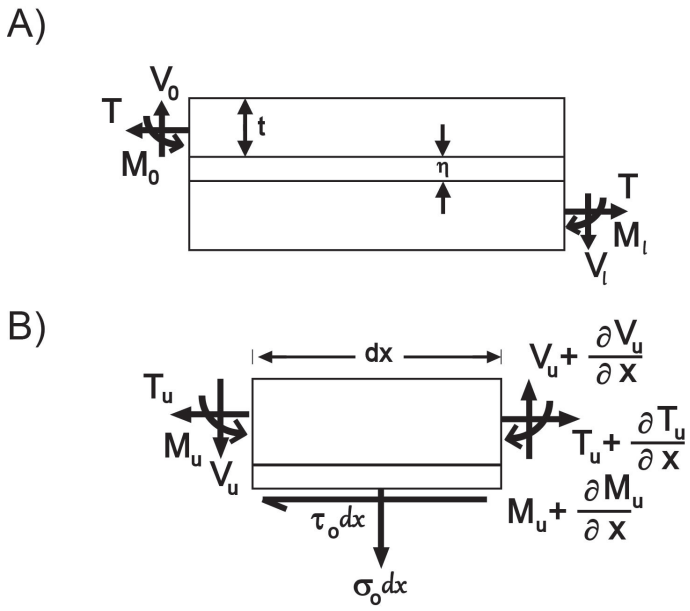

Figure A.2: A)Diagram showing the loading applied on the joint. B) Diagram showing the elements of the analysis in the lap region.

The analysis of the lap region (Figure A.2A) begins with dividing it to upper (u) and lower (l) parts. An assumption is made that the deformation in the adherends is due completely to the longitudinal stress in the x direction in the adherend. By deriving the equilibrium equations of forces in the x and y directions as well as the equilibrium of momentum in the upper adherend (Figure A.2B) we have:

$$\tau_o = \frac{\partial T_u}{\partial x} \tag{A.9}$$

$$\sigma_o = \frac{\partial V_u}{\partial x} \tag{A.10}$$

$$\frac{\partial M_u}{\partial x} - V_u + \tau_o \frac{t}{2} = 0 \tag{A.11}$$

By following the same approach for the lower adherend;

$$\tau_o = -\frac{\partial T_l}{\partial x} \tag{A.12}$$

$$\sigma_o = -\frac{\partial V_l}{\partial x} \tag{A.13}$$

$$\frac{\partial M_l}{\partial x} - V_l + \tau_o \frac{t}{2} = 0 \tag{A.14}$$

From the plate theory the following equations could be written for the vertical displacements v_u and v_l:

$$\frac{d^2 v_u}{dx^2} = -\frac{M_u}{D} \qquad\qquad \frac{d^2 v_l}{dx^2} = -\frac{M_l}{D} \tag{A.15}$$

Where $D = \frac{Et^3}{12(1-\nu^2)}$ refers to the flexural rigidity of the adherends.

The next equations are for the longitudinal displacements (u_u and u_l) of adherends next to the adhesive:

$$\frac{du_u}{dx} = \frac{1}{E}\left(\frac{T_u}{t} - \frac{6M_u}{t^2}\right) \qquad\qquad \frac{du_l}{dx} = \frac{1}{E}\left(\frac{T_l}{t} + \frac{6M_l}{t^2}\right) \tag{A.16}$$

Goland & Reissner [19] neglected the stress variations in the bond-line. Consecutively, the system of equations is completed by the relations by the stresses and strains in the adhesive:

$$\frac{\tau_o}{G_c} = \frac{u_u - u_l}{\eta} \tag{A.17}$$

$$\frac{\sigma_0}{E_c} = \frac{v_u - v_l}{\eta} \tag{A.18}$$

After differentiating Equation A.18 two times, and applying Equation A.15, Equation A.1, and Equation A.2 the first two boundary conditions for the peeling stress in the bond can be written as:

$$\boxed{at \quad x = -c, \qquad \frac{d^2\sigma_o}{dx^2} = \frac{E_c}{\eta}\left(\frac{M_o}{D}\right)} \tag{A.19}$$

$$\boxed{at \quad x = +c, \qquad \frac{d^2\sigma_o}{dx^2} = \frac{E_c}{\eta}\left(\frac{M_o}{D}\right)} \tag{A.20}$$

Similarly, the other two boundary conditions for peeling stress in the bond-line were obtained by differentiating Equation A.18 for three times, and applying Equation A.16, Equation A.1, Equation A.2, Equation A.11, and Equation A.14:

$$\boxed{at \quad x = -c, \qquad \frac{d^3\sigma_o}{dx^3} = -\frac{E_c}{\eta}\left(\frac{V_o}{D}\right)} \tag{A.21}$$

$$\boxed{at \quad x = +c, \qquad \frac{d^3\sigma_o}{dx^3} = \frac{E_c}{\eta}\left(\frac{V_o}{D}\right)} \tag{A.22}$$

A.3 On peeling stresses in SLJs

The objective of this section is to reformulate Goland & Reissner solution to account for Poisson's ratio of adherends on the general solution of the peeling stresses in the bond-line and therefore obtain an expression for it . Furthermore, by comparing solutions derived for peeling (σ_o) and Shear stresses (τ_o) (see Equation A.6 and Equation A.7) it can be seen that only the general solution of the peeling stresses is dependent on the Poission's ratio (ν) of the adherends and therefore could be further modified.
A general solution for Equation A.7 could be written as follows:

$$\sigma_o = B_1 e^{nx}\cos nx + B_2 e^{-nx}\cos nx + B_3 e^{nx}\sin nx + B_4 e^{-nx}\sin nx \tag{A.23}$$

$$\text{Where } n = \sqrt[4]{\frac{6E_c(1-\nu^2)}{t^3 E\eta}}$$

By applying the boundary conditions driven in previous section (Equation A.19-A.22) the general solution for σ_o could be further simplified:

$$\sigma_o = B_1^* \cosh nx \cos nx + B_2^* \sinh nx \sin nx \tag{A.24}$$

Whereas n in Goland & Reissner original solution was defined to be : $n_{GR} = \sqrt[4]{\frac{6E_c}{t^3 E\eta}}$. Figure A.3 demonstrates an example on the effect of adherends' Poisson's ratio on the maximum peeling stress in a SLJ with the following geometrical and mechanical properties:

E=86.9 GPa	E_c=1140 MPa	G_c=428.5 MPa	T=1000 N/m
l=15 cm	c=1.25 cm	t=5 mm	η=0.2 mm

The solutions derived in the example above for the peeling stresses in the bond-line shows that σ_o^{max} only changed slightly for the original Goland & Reissner solution, while changing the adherends' Poisson's ratio from 0 to 0.5. It should be noted that the change from n_{GR} to n is not the only factor that causes difference between the exact value for σ_o in modified and general solutions. Additionally, the exact solution stated in Goland & Reissner paper [19] was found not to satisfy Equation A.7. In contrast, by using modified solution, it is observed that σ_o^{max} decreases about 30% as the Poisson's ratio from increases from 0 to 0.5 (See Figure A.3B).

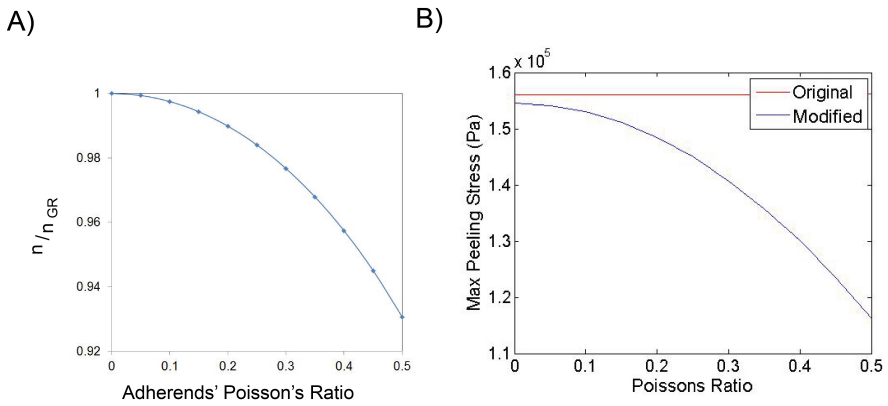

Figure A.3: A) comparison between n and n_{GR} for different adherend ν values.)An example of maximum peeling stress in the bond-line for original and modified Goland & Reissner Solution.

Appendix B

FINITE ELEMENT STUDY OF THE SINGLE LAP JOINT MODEL

Adding carbon fiber fabric in the bond-line significantly changes the stress distribution by changing the effective stiffness and total thickness. In this section, a simple finite element (FE) study was completed to investigate the effect of inclusion heater fabric on the stresses in the bond region.

It will be shown here by using simple linear elastic FE analysis that the maximum stresses decrease as the bond-line gets thicker; In contrast,da Silva et al [69] stated that in practise lap-joint strength increases as the bond-line gets thinner. Furthermore, studies in the past literature have addressed this topic. Crocombe [70] showed with an elastic analysis that the stress distribution of a thin bond-line is more concentrated at the ends of the overlap than a thicker bond-line, which has more uniform stress distribution. Therefore, a thin bond-line will reach the yielding stress at a lower load than a thick bond-line; however, when yielding does occur in a thicker joint, there is less "elastic reserve" to sustain further loading, and thus, yielding spreads more quickly. Moreover, the discrepency can be explained by the fact that thicker bond-lines contain more defects such as voids and microcracks [71].

The models had an overlap length, adherend thickness and bond gap similar to the fabricated specimens in Section 2.2. To simulate the Instron loading, the models were not allowed to move at one direction, while both ends were permitted only to translate axially without rotation, and an axial-direction load was applied.

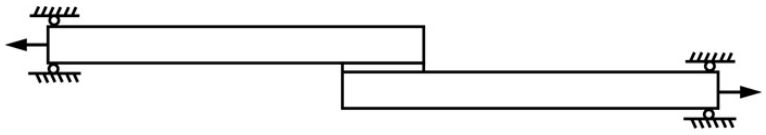

Figure B.1: Boundary condition of the SLJ FE model.

Two-dimensional models of SLJ specimens with different interface configurations were

performed using the commercial finite element package ANSYS. The adherends and adhesives were modeled as isotropic linear elastic materials. The elastic modulus of the adherend and adhesive were taken as $E = 86.9$ GPa and $E_c = 1140$ MPa, respectively. Poissons ratio for both adhesive and adherends was taken as 0.33.

The finite element delivers the stress distribution within the mid-line of the adhesive, denoted here by (σ_o, τ_o). The calculated results of course do not include any effects of large deformation, material nonlinearity, or material and interface failure. They are used primarily for a qualitative ranking of the stress level created by different configurations.

Mesh size can affect the FEM results. Furthermore, a mesh sensitivity study was conducted in order to minimize the model sensitivity to the mesh size. Mesh was refined in the spots closer to the bond area. Figure B.2 shows that the maximum peeling stress is mesh size dependant due to singularity in the interface of the adhesive and adherends.

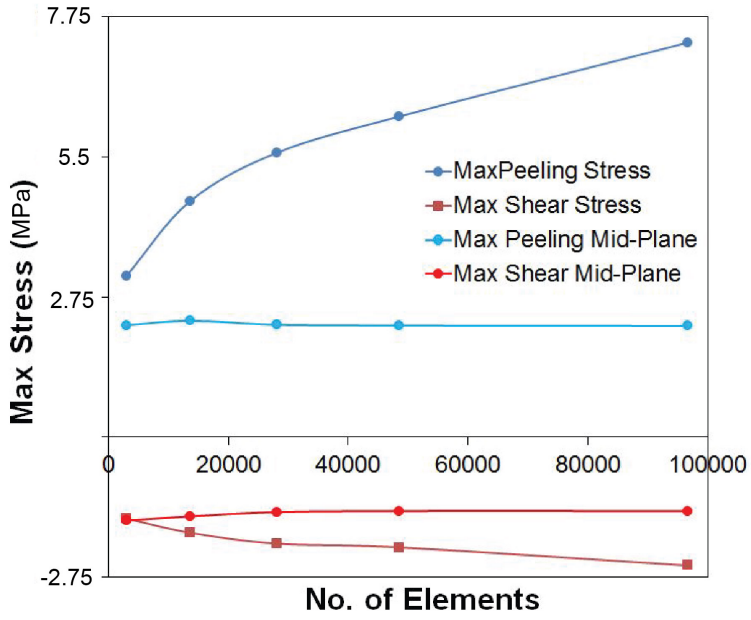

Figure B.2: Mesh sensitivity study of the FE model.

To verify the FE models, a model with concentrated load was produced and no change in the stresses in the mid-bond was observed. As shown on Figure B.3, FE results match well with Goland & Reissner for the example solved in Appendix A; however, the peak stresses

in the FE model does not occur in the edges of the bond area in contrast to Goland & Reissner theoritical model. Detailed linear elastic FE studies were performed to study the

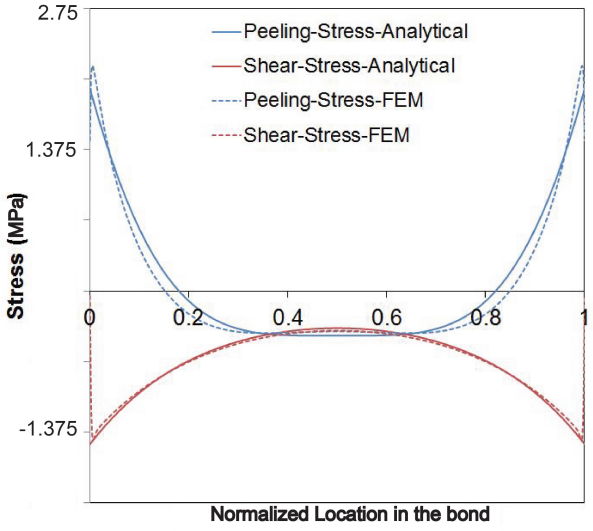

Figure B.3: An example comparing the mid-bond stresses between FE model and Goland & Reissner Solution.

effect of bond thickness on the maximum stresses in the bond-line, and the results were compared to Goland & Reissner anlytical solution. Figure B.4 shows that the maximum stresses decrease as the bond-line gets thicker. Moreover, da Silva et al. [69] addressed the discrepency between FE model and experimental results in their work.

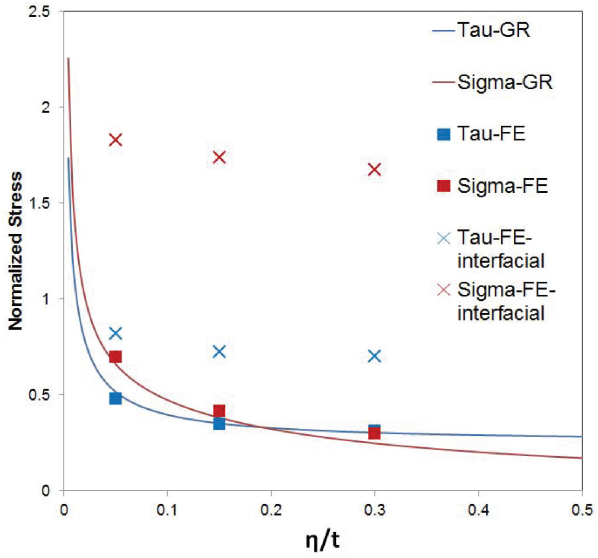

Figure B.4: Effect of changing the bond thickness on the maximum stresses in the mid-bond.

Appendix C

HEAT DIFFUSION EQUATION FOR EMBEDDED RESISTIVE HEATERS

C.1 Derivation of the Heat Diffusion Equation

We define a differential control volume, identify the relevant energy transfer process, and applying the energy conservation requirement [72]. The result is a differential equation whose solution, for prescribed boundary conditions, provides the temperature distribution in the medium.

Consider a homogeneous medium within which there is no bulk motion, and the temperature distribution $T(x, y, z)$ is expressed in Cartesian coordinates. Following the methodology of applying conservation of energy, we first define an infinitesimally small control volume, $dx.dy.dz$ as shown in Figure C.1. The conduction heat rates at the opposite surfaces can then be expressed as a Taylor series expansion where, neglecting the higher order terms:

$$q_{x+dx} = q_x + \frac{\partial q_x}{\partial x} dx \tag{C.1}$$

$$q_{y+dy} = q_y + \frac{\partial q_y}{\partial y} dy \tag{C.2}$$

$$q_{z+dz} = q_z + \frac{\partial q_z}{\partial z} dz \tag{C.3}$$

Heating occurs uniformly within the control volumeand could be expressed in terms of volumetric heat generation rate $\dot{q}(W/m^3)$ where energy generation is due to electric resistance heating:

$$\dot{E}_g = \dot{q} dx dy dz = I^2 R dx dy dz \tag{C.4}$$

where I is the electrical current, and R is the resistance per unit length.

If the material is not experiencing a change in phase, the energy storage term may be expressed as:

$$\dot{E_{st}} = \rho c_p \frac{\partial T}{\partial t} dx dy dz \tag{C.5}$$

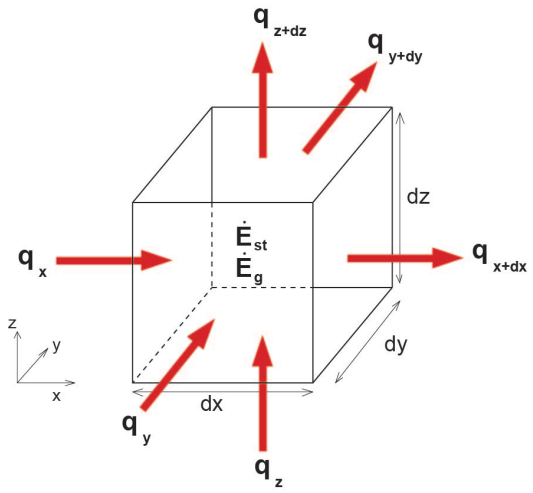

Figure C.1: Differential control volume, $dxdydz$, for conduction analysis in Cartesian coordinates.

On a rate basis, the general form of energy requirement is:

$$\dot{E_{in}} + \dot{E_g} - \dot{E_{out}} = \dot{E_{st}} \tag{C.6}$$

Hence, recognizing that the conduction rates constitute the energy inflow, $\dot{E_{in}}$, and outflow $\dot{E_{out}}$, and substituting Equations C.4 and C.5, we obtain:

$$q_x + q_y + q_z + \dot{q}dxdydz - q_{x+dx} - q_{y+dy} - q_{z+dz} = \rho c_p \frac{\partial T}{\partial t} dxdydz \tag{C.7}$$

Substituting equations C.1,C.2, and C.3, it follows that:

$$-\frac{\partial q_x}{\partial x}dx - \frac{\partial q_y}{\partial y}dy - \frac{\partial q_z}{\partial z}dz + \dot{q}dxdydz = \rho c_p \frac{\partial T}{\partial t} dxdydz \tag{C.8}$$

The conduction heat rates may be evaluated from Fourier's law:

$$q_x = -kdydz\frac{\partial T}{\partial x} \tag{C.9}$$

$$q_y = -kdxdz\frac{\partial T}{\partial y} \tag{C.10}$$

$$q_z = -kdxdy\frac{\partial T}{\partial z} \tag{C.11}$$

In our study, we will be looking at a steady-state condition, therefore, the right hand side of equation C.8 will be zero. Substituting Equations C.9, C.10, and C.11 into Equation C.8, and dicing out the dimensions of the control volume ($dxdydz$), we obtain:

$$\frac{\partial}{\partial x}(k\frac{\partial T}{\partial x}) + \frac{\partial}{\partial y}(k\frac{\partial T}{\partial y}) + \frac{\partial}{\partial z}(k\frac{\partial T}{\partial z}) + I^2R = 0 \tag{C.12}$$

C.2 Boundary Conditions

Equation C is a second order differential equation in three dimensions. Therefore, 6 known boundary conditions are needed to solve this equation for T. To match the experimental measurements presented in Chapter 4, a mixture of two main boundary conditions could be used for the heat diffusion equation as shown on Figure C.2A and Figure C.2B.

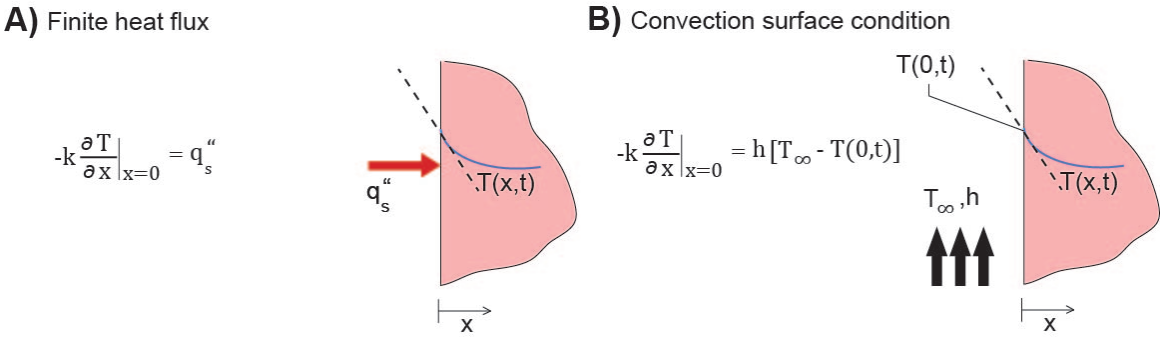

Figure C.2: Boundary conditions for the heat diffusion equation

Appendix D

APPLICATION OF EMBEDDED RESISTIVE HEATING IN CO-BONDING OF COMPOSITE SCARF REPAIRS

In this section, an external heating source (heat blanket) was used in addition to an embedded resistive heater to cure the B-staged repair patch in addition to the thin film adhesive used to repair the composite structure. The meantioned heating method will be reffered to "combined heating" here. The experimental procedures, materials, and methods discussed in Chapter 3 were carefully followed in this section. A schematic of the experimental setup for combined heating in composite scarf repair is presented in Figure D.1. In this study, an emprical approach (dry-run) was used to measure the temperature inside

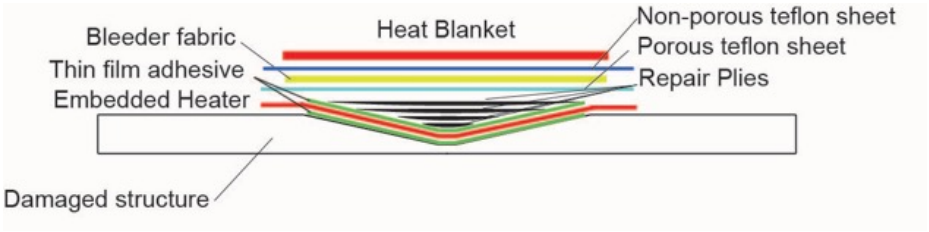

Figure D.1: Schematic of the materials and equipments used for co-bonding a scarf repair patch using combined heating.

the bond-line prior to the repair process. In the dry-run stage, the structural film adhesive used during joining is replaced with (non-adhesive) Teflon electrically insulating sheets to prevent adhesive bonding. After placing the temeparure sensors, 14 plies of B-staged woven graphite-epoxy prepregs that were cut according to the specific ply size and direction it was replacing were placed on the scarfed area. A total number of 16 sensors were used to record temperatures, as shown on Figure D.2.

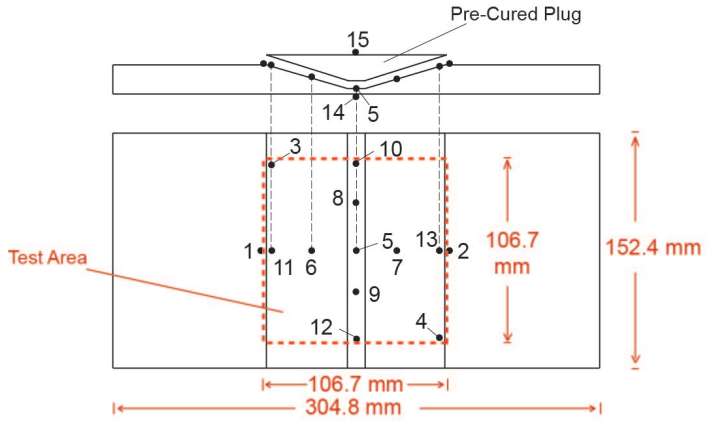

Figure D.2: Schematic of the scarf repair showing the location of the thermocouples in dry-runs.

D.1 An emprical approach (dry-run) to measure temperatures in a co-bonded repair

D.1.1 Temperature distribution across a B-staged composite repair patch

In practice, heat flux needs to pass a couple of layers of fabrics in addition to the repair material to reach to the bond area. This results in a through thickness thermal gradients, which leads to over-heating the durface of the repair material adjacent to the external heater. In this section, through thickness temperature gradients was measured at 4 points, and is shown on Figure D.3. This figures show that combined heating technique leads to a more uniform through thickness temperatures in the repair patches. More unidorm temperatures across the repair area could lead to a lower thermal stresses in the repair patch, and thereby reinforcing the repaired structure.

D.1.2 Temperature uniformity in the bond area

Figure D.4 shows the temperature data feedback recorded by all eleven thermocouples embedded in the bond-line for all of the heating techniques. Results showed that the measure in bond temperature differences for all three heating methods were relatively close, and within 4% of the cure temperature.

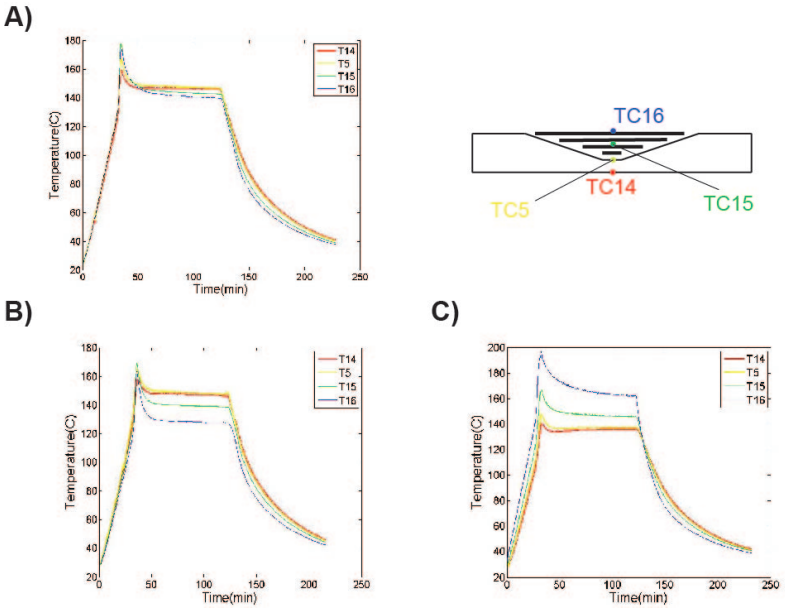

Figure D.3: Temperature feedback from the thermocouples located through the thickness of the scarf repairs in the A) Combined heating B) Embedded resistive heating C) External Heating

D.1.3 Tensile strength of scarf repair joints

As shown in Figure D.5, scarf repairs cured through combined heating had the highest average cure % among all of the heating methods. However, those tensile samples had the lowest average tensile strength. The residual stresses as a result of curing the repair patches are present after the curing process, and potentially could further weaken the tensile strength of the scarf repairs in case they are in the same direction of the tensile loading. Compression testing are required in order to verify this hypothesis.

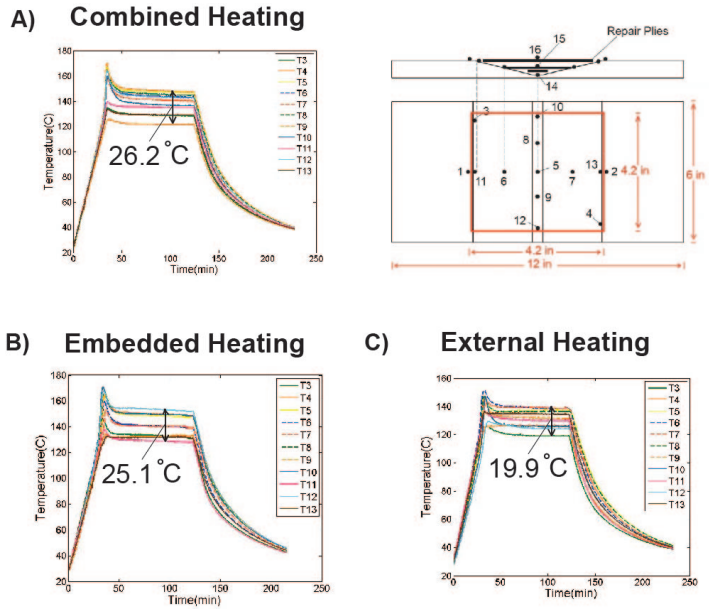

Figure D.4: Temperature feedback from the thermocouples located in the bond-line of the scarf repairs in the A) Combined heating B) Embedded resistive heating C) External Heating

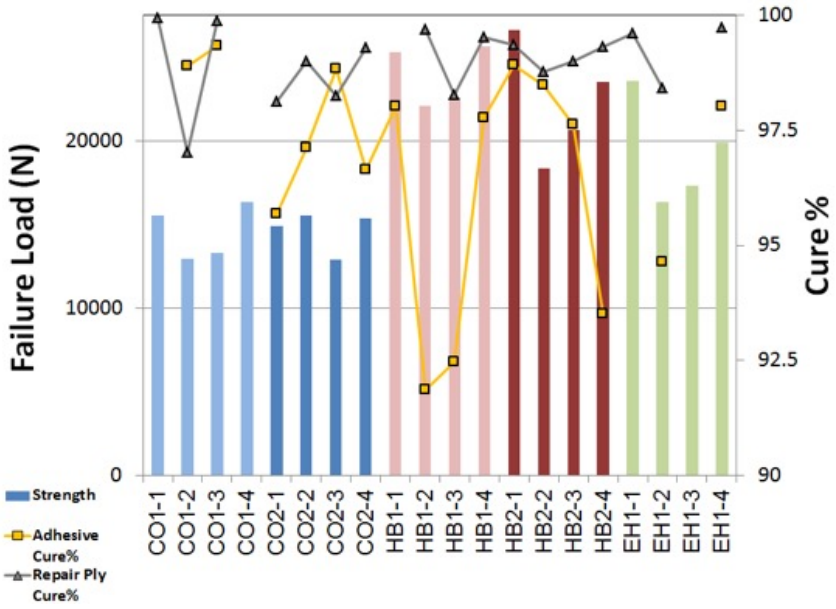

Figure D.5: Tensile strength and DSC results for Combined Heating (CO), Embedded Resistive Heating (EH), and External Heating (HB)

BIBLIOGRAPHY

[1] Michaela D Platzer. Us aerospace manufacturing: Industry overview and prospects. DTIC Document, 2009.

[2] Janet L Sawin, Eric Martinot, Virginia Brien, Angus McCrone, Jodie Roussell, Douglas Barnes, Christopher Flavin, Lisa Mastny, Diana Kraft, Shannon Wang, et al. Renewables 2010-global status report. 2010.

[3] George Marsh. The challenge of composite fuselage repair. *Reinforced Plastics*, 56(3):30 – 35, 2012.

[4] Maxwell Davis and David Bond. Principles and practices of adhesive bonded structural joints and repairs. *International Journal of Adhesion and Adhesives*, 19(23):91 – 105, 1999.

[5] M. Ashrafi, S. Devasia, and M. E. Tuttle. Resistive embedded heating for homogeneous curing of adhesively bonded joints. *International Journal of Adhesion and Adhesives*, 2014.

[6] S. Mahdi, H.-J. Kim, B. A. Gama, S. Yarlagadda, and J. W. Gillespie. A comparison of oven-cured and induction-cured adhesively bonded composite joints. *Journal of Composite Materials*, 37(6):519–542, 2003.

[7] A. N. Rider, C. H. Wang, and J. Cao. Internal resistance heating for homogeneous curing of adhesively bonded repairs. *International Journal of Adhesion and Adhesives*, 31(3):168–176, 2011.

[8] K. B. Katnam, L. F. M. Da Silva, and T. M. Young. Bonded repair of composite aircraft structures: A review of scientific challenges and opportunities. *Progress in Aerospace Sciences*, 61(0):26–42, 2013.

[9] V. P. Rajan, M. N. Rossol, and F. W. Zok. Optimization of digital image correlation for high-resolution strain mapping of ceramic composites. *Experimental Mechanics*, 52(9):1407–1421, 2012.

[10] M. Sato, A. Toshimitsu Yokobori, Yoshihito Ozawa, Takayuki Kamiyama, Toshiaki Miyanaga, P. W. R. Beaumont, and Hideki Sekine. Experimental study of repair efficiency for single-sided composite patches bonded to aircraft structural panels. *Advanced Composite Materials*, 11(1):51–59, 2002.

[11] B. Egan, C.T. McCarthy, M.A. McCarthy, P.J. Gray, and R.M. OHiggins. Static and high-rate loading of single and multi-bolt carbonepoxy aircraft fuselage joints. *Composites Part A: Applied Science and Manufacturing*, 53(0):97 – 108, 2013.

[12] GarthM. Pearce, AlastairF. Johnson, RodneyS. Thomson, and DonaldW. Kelly. Experimental investigation of dynamically loaded bolted joints in carbon fibre composite structures. *Applied Composite Materials*, 17(3):271–291, 2010.

[13] Aijuan Gu and Guozheng Liang. Preparation and properties of a novel high-performance resin system with low injection temperature for resin transfer moulding. *Polymer International*, 53(9):1388–1393, 2004.

[14] Pavel Simacek, Suresh G. Advani, and Stanley A. Iobst. Modeling flow in compression resin transfer molding for manufacturing of complex lightweight high-performance automotive parts. *Journal of Composite Materials*, 42(23):2523–2545, 2008.

[15] Sanjay Sharma and Kyle Wetzel. Process development issues of glass-carbon hybrid-reinforced polymer composite wind turbine blades. *Journal of Composite Materials*, 2009.

[16] Toshiyuki Shimokawa, Yoshiaki Kakuta, Daisuke Saeki, and Yoshiyasu Kogo. Carbon plain-weave fabric low-temperature vacuum cure epoxy composite: Static and fatigue strength at room and high temperatures and practicality evaluation. *Journal of Composite Materials*, 41(18):2245–2265, 2007.

[17] Venkatagireesh Menta, Ramabhadraraju Vuppalapati, K Chandrashekhara, Thomas Schuman, and Jilun Sha. Elevated-temperature vacuum-assisted resin transfer molding process for high performance aerospace composites. *Polymer International*, 62(10):1465–1476, 2013.

[18] M. Ashrafi, B. P. Smith, S. Devasia, and M. E. Tuttle. Embedded resistive heating in composite scarf repairs. *Composites - Part A*, Submitted.

[19] M Goland and E Reissner. The stresses in cemented joints. *Journal of Applied Mechanics*, pages A17–A27, 1944.

[20] Stefano Turri, Aldo Sanguineti, and Romina Lecchi. Novel glass fiber-reinforced composites having a uv and peroxy curable fluoropolymer matrix. *Macromolecular Materials and Engineering*, 288(9):708–716, 2003.

[21] Thierry Glauser, Mats Johansson, and Anders Hult. A comparison of radiation and thermal curing of thick composites. *Macromolecular Materials and Engineering*, 274(1):25–30, 2000.

[22] C. Nightingale and R. J. Day. Flexural and interlaminar shear strength properties of carbon fibre/epoxy composites cured thermally and with microwave radiation. *Composites Part A: Applied Science and Manufacturing*, 33(7):1021–1030, 2002.

[23] Varaporn Tanrattanakul and Dumrong Jaroendee. Comparison between microwave and thermal curing of glass fiberepoxy composites: Effect of microwave-heating cycle on mechanical properties. *Journal of Applied Polymer Science*, 102(2):1059–1070, 2006.

[24] T. J. Ahmed, D. Stavrov, H. E. N. Bersee, and A. Beukers. Induction welding of thermoplastic compositesan overview. *Composites Part A: Applied Science and Manufacturing*, 37(10):1638–1651, 2006.

[25] Dilmurat Abliz, Duan Yugang, Leif Steuernagel, Xie Lei, Li Dichen, and Gerhard Ziegmann. Curing methods for advanced polymer composites - a review. *Polymers&.Polymer Composites*, 21(6):341–348, 2013.

[26] R. Carbas, G. Viana, L. da Silva, and G. Critchlow. Functionally graded adhesive patch repairs of wood beams in civil applications. *Journal of Composites for Construction*, 0(0):11, 2014.

[27] B. Ramakrishnan, L. Zhu, and R. Pitchumani. Curing of composites using internal resistive heating. *Journal of Manufacturing Science and Engineering*, 122(1):124–131, 1999. 10.1115/1.538913.

[28] Dennis Butler and Renata S Engel. On the use of embedded graphite patches for cure in resin transfer molding. In *Proceedings, ICCM-10*, volume 3, pages 269–275, 1995.

[29] Liwen Zhu and Ranga Pitchumani. Processing envelopes for supplemental internal resistive heating during thermosetting composites cure. *Journal of reinforced plastics and composites*, 18(13):1242–1253, 1999.

[30] Stephen A Sarles and Donald J Leo. Consolidation of u-nyte® epoxy-coated carbon-fiber composites via temperature-controlled resistive heating. *Journal of Composite Materials*, 42(24):2551–2566, 2008.

[31] Yizhuo Gu, Xing Qin, Min Li, Kaomin Zhang, and Zuoguang Zhang. Temperature distribution and curing behaviour of carbon fibre/epoxy composite during vacuum assisted resin infusion moulding using rapid heating methods. *Polymers & Polymer Composites*, 23(1):11, 2015.

[32] Jeonyoon Lee, Itai Y Stein, Seth S Kessler, and Brian L Wardle. Aligned carbon nanotube film enables thermally induced state transformations in layered polymeric materials. *ACS applied materials & interfaces*, 7(16):8900–8905, 2015.

[33] Christopher Joseph and Christopher Viney. Electrical resistance curing of carbon-fibre/epoxy composites. *Composites Science and Technology*, 60(2):315–319, 2000.

[34] Carlo Santos, Thomas Plaisted, Diego Arbelaez, and Siavouche Nemat-Nasser. Modeling and testing of temperature behavior and resistive heating in a multifunctional composite. volume 5387, pages 24–26. 10.1117/12.537654.

[35] L. Zhu and R. Pitchumani. Analysis of a process for curing composites by the use of embedded resistive heating elements. *Composites Science and Technology*, 60(14):2699–2712, 2000.

[36] Simon A Hayes, Austin D Lafferty, Gader Altinkurt, Peter R Wilson, Matthew Collinson, and P Duchene. Direct electrical cure of carbon fiber composites. *Advanced Manufacturing: Polymer & Composites Science*, 1(2):112–119, 2015.

[37] Hiroshi Fukuda. Processing of carbon fiber reinforced plastics by means of joule heating. *Advanced Composite Materials*, 3(3):153–161, 1994.

[38] Eric C Eveno, John W Gillespie, et al. Resistance welding of graphite polyetheretherketone composites: an experimental investigation. *Journal of Thermoplastic Composite Materials*, 1(4):322–338, 1988.

[39] Brandon P Smith, Mahdi Ashrafi, Mark E Tuttle, and Santosh Devasia. Bondline temperature control for joining composites with an embedded heater. *Journal of Manufacturing Science and Engineering*, 138(2):021011, 2016.

[40] Bartolom Mas, Juan P. Fernndez-Blzquez, Jonathan Duval, Humphrey Bunyan, and Juan J. Vilatela. Thermoset curing through joule heating of nanocarbons for composite manufacture, repair and soldering. *Carbon*, 63(0):523–529, 2013.

[41] Ping-Cheng Sung and Shih-Chin Chang. The adhesive bonding with buckypaper–carbon nanotube/epoxy composite adhesives cured by joule heating. *Carbon*, 91:215–223, 2015.

[42] C. L. Brett. The effect of state of cure on bond performance for an epoxy resin system. *Journal of Applied Polymer Science*, 20(6):1431–1440, 1976.

[43] R.A. Fava. Differential scanning calorimetry of epoxy resins. *Polymer*, 9(0):137 – 151, 1968.

[44] Mahdi Ashrafi, Amin Ajdari, Nima Rahbar, Jim Papadopoulos, Hamid Nayeb-Hashemi, and Ashkan Vaziri. Adhesively bonded single lap joints with non-flat interfaces. *International Journal of Adhesion and Adhesives*, 32(0):46–52, 2012.

[45] RL Vijaya Kumar, MR Bhat, and CRL Murthy. Experimental analysis of composite single-lap joints using digital image correlation and comparison with theoretical models. *Journal of Reinforced Plastics and Composites*, 32(23):1858–1876, 2013.

[46] Bing Pan, Kemao Qian, Huimin Xie, and Anand Asundi. Two-dimensional digital image correlation for in-plane displacement and strain measurement: a review. *Measurement Science and Technology*, 20(6):1–17, 2009.

[47] Mahdi Ashrafi and Mark Tuttle. *High Strain Gradient Measurements in Notched Laminated Composite Panels by Digital Image Correlation*, volume 4, pages 75–81. Springer International Publishing, 2014.

[48] M.A. Sutton, J.J. Orteu, and H.W. Schreier. *Image Correlation for Shape, Motion and Deformation Measurements: Basic Concepts, Theory and Applications*. Springer London, Limited, 2009.

[49] MS Found and MJ Friend. Evaluation of cfrp panels with scarf repair patches. *Composite structures*, 32(1):115–122, 1995.

[50] Mathieu Prau and Pascal Hubert. Processing of co-bonded scarf repairs: Void reduction strategies and influence on strength recovery. *Composites Part A: Applied Science and Manufacturing*, 84:236 – 245, 2016.

[51] Henrik Schmutzler, Jan Popp, Edwin Bchter, Hans Wittich, Karl Schulte, and Bodo Fiedler. Improvement of bonding strength of scarf-bonded carbon fibre/epoxy laminates by nd:yag laser surface activation. *Composites Part A: Applied Science and Manufacturing*, 67:123 – 130, 2014.

[52] Seyedmohammad S. Shams and Rani F. El-Hajjar. Overlay patch repair of scratch damage in carbon fiber/epoxy laminated composites. *Composites Part A: Applied Science and Manufacturing*, 49:148 – 156, 2013.

[53] R.D.S.G. Campilho, M.F.S.F. de Moura, A.M.G. Pinto, J.J.L. Morais, and J.J.M.S. Domingues. Modelling the tensile fracture behaviour of {CFRP} scarf repairs. *Composites Part B: Engineering*, 40(2):149 – 157, 2009.

[54] Y. Q. Wang, M. A. Sutton, H. A. Bruck, and H. W. Schreier. Quantitative error assessment in pattern matching: Effects of intensity pattern noise, interpolation, strain and image contrast on motion measurements. *Strain*, 45(2):160–178, 2009.

[55] Elena E Antonova and David C Looman. Finite elements for thermoelectric device analysis in ansys. In *Thermoelectrics, 2005. ICT 2005. 24th International Conference on*, pages 215–218. IEEE, 2005.

[56] Omer Soykasap, Sukru Karakaya, Yelda Akcin, and Mehmet Colakoglu. Finite element modelling of cnt-doped cfrp plates for lightning strike damage. In *Smart Intelligent Aircraft Structures (SARISTU)*, pages 825–837. Springer, 2016.

[57] Toshio Ogasawara, Yoshiyasu Hirano, and Akinori Yoshimura. Coupled thermal-electrical analysis for carbon fiber composites exposed to simulated lightning current. *Journal of the Japan Society for Aeronautical and Space Sciences*, 57(667):336–343, 2009.

[58] Omer Soykasap, Sukru Karakaya, and Mehmet Colakoglu. Simulation of lightning strike damage in carbon nanotube doped cfrp composites. *Journal of Reinforced Plastics and Composites*, page 0731684415618458, 2015.

[59] X Sun and P Dong. Analysis of aluminum resistance spot welding processes using coupled finite element procedures. *WELDING JOURNAL-NEW YORK-*, 79(8):215–S, 2000.

[60] NT Williams and JD Parker. Review of resistance spot welding of steel sheets part 1 modelling and control of weld nugget formation. *International Materials Reviews*, 49(2):45–75, 2004.

[61] Zhigang Hou, Ill-Soo Kim, Yuanxun Wang, Chunzhi Li, and Chuanyao Chen. Finite element analysis for the mechanical features of resistance spot welding process. *Journal of Materials Processing Technology*, 185(1):160–165, 2007.

[62] HS Cho and YJ Cho. A study of the thermal behavior in resistance spot welds. *Welding Journal*, 68(6):236s–244s, 1989.

[63] Dale Cigoy. Accurate low-resistance measurements start with identifying sources of error. *Cleveland: KEITHLEY INSTRUMENTS, INC*, 2010.

[64] Lit S Han and William F Boyee. Thermal conductivities and diffusivities of graphite-epoxy composites. Technical report, DTIC Document, 1983.

[65] Thomas Kruse. Bonding of cfrp primary aerospace structures. Technical report, CFK Valley Stade Convention, 2013.

[66] Michael J. Hoke. Adhesive bonding of composites. Technical report, Abaris Training Inc., 2005.

[67] K. DEB. *Optimization for engineering design: Algorithms and Examples*. PHI Learning, 2012.

[68] LFM da Silva and RFT Lima. Closed-form solutions for adhesively bonded joints, 2008.

[69] Lucas FM da Silva, TNSS Rodrigues, MAV Figueiredo, MFSF De Moura, and JAG Chousal. Effect of adhesive type and thickness on the lap shear strength. *The journal of adhesion*, 82(11):1091–1115, 2006.

[70] A.D. Crocombe. Global yielding as a failure criterion for bonded joints. *International Journal of Adhesion and Adhesives*, 9(3):145 – 153, 1989.

[71] R D Adams and N A Peppiatt. Stress analysis of adhesive-bonded lap joints. *The Journal of Strain Analysis for Engineering Design*, 9(3):185–196, 1974.

[72] Frank Incropera and David DeWitt. Introduction to heat transfer. 1985.